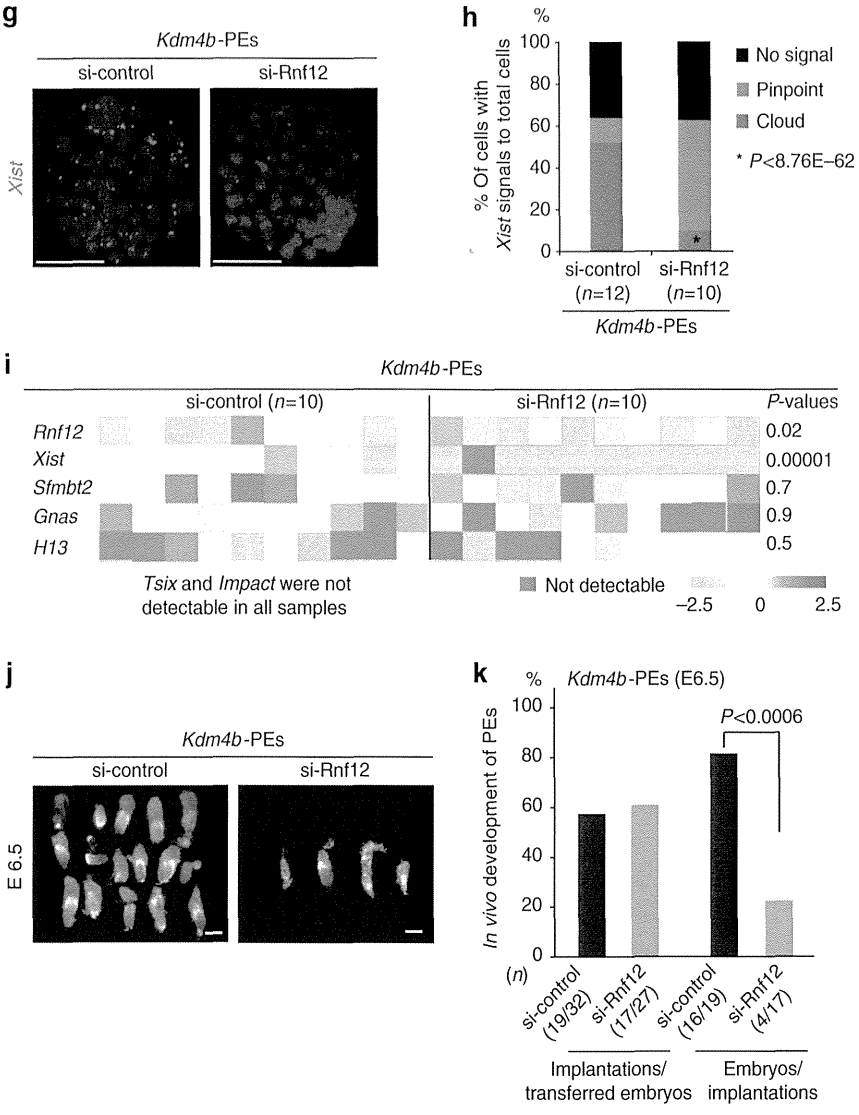

Figure 5 | Loss of Xm-XCI is the primary cause of developmental failure immediately after implantation in most PEs. (**a**) IF combined with FISH analysis of blastocysts in *Egfp*-PEs (upper panel) and *Kdm4b*-PEs (lower panel). CDX2-positive cells were identified as belonging to the trophectoderm (TE). Representative pictures of Z-sections. 4′,6-diamidino-2-phenylindole (DAPI) (blue), CDX2 (green), *Xist* (red) and H3K27me3 (white). Scale bars, 20 μm. The rates of cells with *Xist* (left) or H3K27me3 (right) in the inner cell mass (ICM) (**b**) and TE (**c**), respectively. *n*, number of embryos analysed. The number of cells analysed is shown in Supplementary Table 7. $^{*}P<4.3\times10^{-23}$ (Fisher's exact test). (**d**) Expression states and clustering analysis of imprinted genes. *Sfmbt2* important for placentation and differentially expressed genes (asterisk) are shown. The scale bar indicates normalized values of $\log_2$. (**e**) Embryos with extra-embryonic tissues at E6.5 and E9.5 for *Kdm4b*- and *Egfp*-PEs, respectively. Upper and lower images indicate *Egfp*- and *Kdm4b*-PEs, respectively. Left and right column sides show E6.5 and E9.5, respectively. Scale bars, 200 μm (E6.5) and 500 μm (E9.5). (**f**) Summary of the developmental abilities of *Kdm4b*-PEs and *Egfp*-PEs at postimplantation stages (E6.5 and E9.5). Five and 12 independent recipients were analysed at E6.5 and E9.5, respectively. (**g**,**h**) *Xist* analysis in *Rnf12*-knockdown and control *Kdm4b*-PEs. Representative images of FISH analysis. Scale bars, 50 μm (**g**) and *Xist* expression states (**h**). (**i**) Expression of imprinted and X-linked genes in *Rnf12*-knockdown and control *Kdm4b*-PEs. *P*-values were determined using Student's *t*-tests. (**j**) Embryos with extra-embryonic tissues at E6.5 in *Rnf12*-knockdown and control *Kdm4b*-PEs. Scale bars, 200 μm. (**k**) Summary of the developmental ability of *Rnf12*-knockdown and control *Kdm4b*-PEs at E6.5. Five independent recipients were analysed. The *P*-values were determined using Fisher's exact test.

levels of the promoter region in *Kdm4b*-PEs were significantly reduced, as follows: 5′-R, *Kdm4b*-PEs: 0.84% versus *Egfp*-PEs: 11.48%, $P<0.05$, Student's *t*-tests; XP, *Kdm4b*-PEs: 3.13% versus *Egfp*-PEs: 16.08%; $P<0.04$, Student's *t*-tests; and RA, *Kdm4b*-PEs: 20.16% versus *Egfp*-PEs: 29.99%; Fig. 4g. Taken together, these results demonstrated that H3K9me3 at the promoter region protected Xm-*Xist*, preventing RNF12-mediated activation from the four-cell stage. We concluded that silencing of Xm-*Xist* by imprinting to establish iXCI involved H3K9me3.

Maternal repressive H3K9me3 mark is absent in ES cells. Previous studies have shown that *Xist* is ectopically expressed in embryos cloned from somatic and ES cells[27,28]. However, the cause of aberrant *Xist* expression in cloned embryos remains unknown. Given that high H3K9me3 levels at the promoter region in PEs are lost during development (Fig. 4d,e), we investigated whether the maternal repressive H3K9me3 mark was lost in ES cells and whether *Xist* in ES cells was permissive against RNF12 during oocyte-mediated reprogramming.

To test this possibility, we first examined H3K9me3 states at *Xist* regions in various types of male ES cells, using published data[29,30]. The levels of H3K9me3 at *Xist* regions containing promoters in TT2 and E14 ES cell lines were low compared with those in positive control regions (Supplementary Fig. 9). ChIP-seq analysis revealed that although ectopic expression of KDM4B

in male ES cells induced global H3K9me3 demethylation (Supplementary Fig. 10a–d), it did not alter H3K9me3 levels at *Xist* regions. Moreover, these levels were low compared with those of a known H3K9me3-rich region (Supplementary Fig. 10e)[16]. Furthermore, the expression of *Xist* in cloned embryos was also not affected by ectopic expression of KDM4B (Supplementary Fig. 10f). These results indicated that the maternal repressive H3K9me3 mark was lost.

To establish whether RNF12 is involved in *Xist* activation during oocyte-mediated reprogramming, oocytes treated with si-*Rnf12* were used as recipients for nuclear transfer (Supplementary Fig. 10g). At the four-cell stage, derepression of *Xist* transcription in ES-cloned embryos depended on RNF12 (>50% repression in si-*Rnf12* group; Supplementary Fig. 10h). Taken together, these data indicated that the intrinsic H3K9me3 mark, which was essential for repression of *Xist* by RNF12, was lost during embryo development. This indicated that the primary cause of aberrant *Xist* expression in cloned embryos was involved in loss of intrinsic H3K9me3 at *Xist* regions.

Effects of iXCI disruption on FEs. The effects of Xm-*Xist* derepression on postimplantation development remain unclear. First, we asked whether ectopic *Kdm4b* expression caused Xm-*Xist* derepression in FEs. *Kdm4b*-FEs developed into blastocysts with high efficiency (>80% of two-cell embryos; Supplementary Table 6). At the 96-h blastocyst stage, *Xist* transcription was derepressed in male *Kdm4b*-FEs, while *Pgk1* and *Plac1* levels were reduced to <13% of those observed in controls (Supplementary Fig. 11a). In female *Kdm4b*-FEs, FISH analysis revealed that there were cells with *Xist* biallelic expression (Supplementary Fig. 11b). Although the expression level was slightly elevated (1.3-fold), X-linked genes were also significantly repressed in female *Kdm4b*-FEs (Supplementary Fig. 11c). These results showed that ectopic Xm-*Xist* derepression caused X-linked gene silencing and elimination of iXCI.

To test the effects of iXCI disruption on postimplantation development, we conducted *in vivo* transplantation experiments. Interestingly, our results demonstrated that XCI on Xm during preimplantation did not affect developmental competence to term (*Kdm4b*-FEs: 63.2% versus *Egfp*-FEs: 53.1%; Supplementary Fig. 11d,e), suggesting that aberrant XCI in preimplantation embryos was restored during postimplantation development, probably through an automatic counting function. These results were consistent with the observation that the developmental competency of embryonic cloned embryos was high, despite the ectopic expression of *Xist* and the occurrence of global XCI (Supplementary Fig. 12)[28,31].

Loss of XCI impairs the postimplantation development of PEs. It is still unknown whether the embryonic lethality observed immediately after implantation in the majority of PEs (around 70–80%) can be attributed to the loss of dysregulation of X-linked genes or to loss of expression of autosomal paternally imprinted genes. Figure 2 showed that the percentage of *Xist*-positive cells in *Kdm4b*-PEs was significantly higher than that in *Egfp*-PEs. Thus, we reasoned that *Kdm4b*-PEs would be suitable for studying this long-standing question.

We first performed a detailed analysis of Xm-XCI states in *Kdm4b*-PEs using IF against H3K27me3 and CDX2, a marker of the trophectoderm, in combination with *Xist* FISH, at the blastocyst stage. This analysis revealed that *Xist*-positive cells were significantly increased in the trophectoderm of *Kdm4b*-PEs, although the ratio of H3K27me3-positive cells was comparable to that of *Egfp*-PEs (Fig. 5a–c and Supplementary Table 7). However, no significant difference was observed in the inner cell mass between groups (Fig. 5a–c and Supplementary Table 7), indicating that loss of H3K9me3 in the maternal genome led to establishment of Xm-XCI as an imprinted Xp-XCI.

Next, we carried out transcriptome analysis in *Egfp*-PEs, *Kdm4b*-PEs and FEs using microarray. Clustering analysis based on gene expression patterns showed that all three groups could be distinguished clearly from each other (Supplementary Fig. 13a). Comparison of transcripts between *Egfp*-PEs and *Kdm4b*-PEs identified transcripts that were significantly differentially expressed: 671 transcripts were upregulated and 711 transcripts were downregulated ($P<0.05$, Student's *t*-test and >1.5-fold changes in *Kdm4b*-PEs). Chromosome distribution analysis showed that upregulated transcripts in *Kdm4b*-PEs were distributed across various chromosomes (2.33–7.23%; Supplementary Fig. 13b). However, downregulated transcripts in *Kdm4b*-PEs were mostly concentrated on the X chromosome, which particularly involved the *Xlr* and *Magea* families (10.26%; Supplementary Fig. 13c–e).

Comparison of the imprinted genes between *Egfp*- and *Kdm4b*-PEs revealed that only six genes were significantly differentially expressed (paternally expressed genes: *Impact* and *Fthl17*; maternally expressed genes: *Gnas*, *H13*, *Xlr3b* and *Xlr4b*; Fig. 5d). Clustering analysis based on the expression of imprinted genes showed that the expression levels in *Kdm4b*-PEs were similar to those in *Egfp*-PEs rather than to those of biparental embryos (Fig. 5d). Thus, H3K9me3 demethylation does not result in restoration of expression states in paternally expressed genes.

We conducted *in vivo* transplantation experiments using *Kdm4b*-PEs. Surprisingly, at E6.5, the developmental rates of *Kdm4b*-PEs were markedly increased compared with those of *Egfp*-PEs (*Kdm4b*-PEs: 90% versus *Egfp*-PEs: 35%; $P<0.001$, Fisher's exact test; Fig. 5e,f). At E9.5, although the stages of the recovered embryos varied, *Kdm4b*-PEs retained a significantly higher developmental ability compared with controls (*Kdm4b*-PEs: 64.3% versus *Egfp*-PEs: 31.9%; $P<0.002$, Fisher's exact test; Fig. 5e,f).

However, we did not rule out the possibility that the significant improvement in *Kdm4b*-PE development resulted from restoration of the expression levels of some imprinted genes. To determine whether the improvement in developmental competency could be attributed to the gain of XCI, we constructed *Kdm4b* + si-*Rnf12*-PEs. In *Kdm4b*-PEs with si-*Rnf12* at the blastocyst stage, *Xist* expression analysis by FISH revealed that *Xist* cloud signals in control *Kdm4b*-PEs were present in 51.9% of cells, while those in *Rnf12*-knockdown *Kdm4b*-PEs were present in only 10% of cells, and most of the signals were pinpoint rather than cloud (Fig. 5g,h and Supplementary Table 8).

qPCR analysis showed that although *Xist* signals were significantly reduced in *Kdm4b*-PEs with si-*Rnf12* (12.5% of the control on average), the expression levels of *Impact*, *H13* and *Gnas*, which are expressed in response to ectopic *Kdm4b* expression (Fig. 5d), did not change when compared with those of controls (Fig. 5i). We further demonstrated that RNF12 depletion did not affect *Tsix* and *Sfmbt2* expression levels in *Kdm4b*-PEs (Fig. 5i). These results clearly indicated that RNF12 depletion led to *Xist* downregulation in *Kdm4b*-PEs, without altering the features of PEs.

Finally, *in vivo* transplantation experiments demonstrated that *Xist* repression by RNF12 depletion significantly inhibited developmental competency at E6.5 in *Kdm4b*-PEs (*Kdm4b* + si-control: 84.2% versus *Kdm4b* + si-*Rnf12*: 23.5%; $P<0.0006$, Fisher's exact test; Fig. 5j,k). Taken together, these results demonstrated that the developmental defects seen in PEs immediately after implantation could be attributed to the lack of XCI, but not to loss of expression of paternally expressed genes.

Discussion

In this study, we demonstrated that maternal imprinting of Xm, which protected against *Xist* activation by RNF12 in the preimplantation stages, was mediated by H3K9me3.

Xm-*Xist* imprints are established during oogenesis and autosomal imprinting also occur in the phases[6,10]. In many imprinted genes, DNA methylation at the promoter regions is the primary regulator and H3K9me3 modifications overlap with these regions[32]. However, it is not clear why Xm-*Xist* regions are targeted by H3K9me3, but not by DNA methylation. One of the possibilities is that during primordial germ cell development, *Xist* must be silenced to activate the inactivated allele before inducing the expression of *Dnmt3a/3l*, which encodes a *de novo* DNA methyltransferase that is activated during oogenesis[33]. Consistent with this concept, *Xist* repression begins in primordial germ cells at E10.5 (ref. 34). Thus, comparison of H3K9me3 states at promoter regions in non-growing oocytes with those in growing oocytes will greatly facilitate understanding of the molecular mechanisms of iXCI.

We found that *Kdm4b*-, *Egfp* + TSA- and *Kdm4b* + TSA-PEs did not show complete XCI at the blastocyst stage as compared with female FEs. These results suggested that other repressive marks were imposed on Xm to silence Xm-*Xist* expression. Alternatively, removal of H3K9me3 may be incomplete because demethylation at RA regions was mild (Fig. 4g). However, it is not clear why RA regions show resistance against demethylation by KDM4B. As suggested in a previous study, this mechanism may be related to the three-dimensional structure of the A-repeat, which has been reported to constitute stable regions in the *Xist* transcript[35]. Further studies using ChIP-seq and/or chromatin-conformation capture sequencing technologies in preimplantation embryos are required for comprehensive understanding of *Xist* regulation.

In ES cells, RNF12 induces *Xist* expression through degradation of REX1, which is required for suppression of *Tsix*[36]. Interestingly, we did not detect *Tsix* expression from the morula to the blastocyst stages in *in vitro*-fertilized (IVF) embryos, implying that the molecular mechanism of RNF12-mediated *Xist* activation differs between imprinted and randomly induced XCI. It is not known whether the role of RNF12 in *Xist* activation during the preimplantation stages was direct or indirect. Recent RNF12 studies reported the specific binding of RNF12 to *Smad7* in mouse ES cells[37], suggesting that signalling via transforming growth factor-β family members may be associated with imprinted *Xist* activation.

In this study, we revealed the molecular mechanisms underlying imprinting of XCI and demonstrated the role of XCI in various types of embryo development in mice. Recent studies using somatic- and ES-cloned embryos revealed that aberrant *Xist* reprogramming is a major cause of developmental failure in cloned embryos[27,28]. We found that RNF12 was highly expressed in oocytes compared with somatic and ES cells (>80-fold). Moreover, we showed that H3K9me3 levels at *Xist* promoter regions were low in ES cells and that *Xist* expression in ES-cloned embryos depended on RNF12. These data provided the first evidence that RNF12 inhibited developmental reprogramming. Therefore, the use of RNF12-depleted oocytes as recipient cells would improve cloning efficiency. However, *Xist* activation in cloned embryos may be induced by factors other than RNF12, as supported by the observation that *Xist* was still expressed at ~40% of control levels, even after marked depletion of RNF12. Consistent with this notion, a recent study has demonstrated that RNF12 is dispensable for random XCI *in vivo*[38].

Xm-*Xist* derepression from the four-cell stage could rescue developmental defects in PEs. This finding demonstrated that the primary cause of developmental failure immediately after implantation was a lack of XCI, but not a lack of expression of paternally imprinted genes. We also tested whether *Kdm4b*-PEs could extend development; however, we did not observe extended *Kdm4b*-PE development after E9.5, implying that expression of paternally imprinted genes is required for subsequent development in PEs[11,12].

Our data resolved several long-standing unanswered questions about XCI during preimplantation in various types of embryos (Supplementary Fig. 14). Moreover, given that injection of *Kdm4b* mRNA into PEs improved their developmental ability, genetic mutation leading to embryonic lethality could be rescued by transient expression of epigenomic modifiers during preimplantation phases.

Methods

Embryo manipulations. All mice were maintained and used in accordance with the Guidelines for the Care and Use of Laboratory Animals of the Japanese Association for Laboratory Animal Science and the National Research Institute for Child Health and Development (NRICHD) of Japan. All animal experiments were performed according to protocols approved by the Institutional Animal Care and Use Committee of the NRICHD (Permit Number: A2006-009).

Adult female B6D2F1 mice were purchased from Clea Japan (Tokyo, Japan) and oocytes were collected following standard methods[27]. PEs were generated using Ca-free M16 medium containing 8 mM $SrCl_2$ and Cytochalasin B (5 μg ml^{-1}) (Sigma-Aldrich, St Louis, MO, USA), and cultured KSOM (EMD Millipore, Darmstadt, Germany). Injection experiments (mRNA, short interfering RNA (siRNA) and nuclear transfer) were conducted using a Prime Tech Piezo drive (Sutter Instrument Company, Novato, CA, USA). To produce cloned embryos, nuclear-transferred oocytes were parthenogentically activated. Manipulated embryos were cultured to the developmental stages, as follows: 4-cell, 48 h; morula, 72 h; and blastocyst, 96 and 120 h after parthenogenetic activation or ICSI, respectively. All embryos were cultured at 37 °C in KSOM in an atmosphere containing 5% CO_2. In the TSA experiment, the embryos were cultured for 24 h in activation and culture media containing 50 nM TSA (Sigma-Aldrich). IVF fertilization and nuclear transfer were performed following published procedures[27]. To determine the effects of ectopic KDM4B expression on *Xist* expression in cloned embryos, doxycycline was added to ES cell culture and KSOM medium to a final concentration of 2 μg ml^{-1}. Pseudopregnant ICR mice (Clea Japan) were used as embryo recipients. At E6.5, E9.5 and E18.5, the embryos were recovered from the uterus.

***In vitro* mRNA synthesis.** The coding region of *Kdm3a* was amplified from mouse testis complementary DNA using PCR with KOD-Plus-Neo DNA polymerase (Toyobo, Osaka, Japan). Forward and reverse primers contained T7 promoter and poly(T)$_{120}$ sequences, respectively. A step-down PCR amplification method was used, following the manufacturer's instructions (Toyobo). Poly(A)-containing PCR products were subjected to *in vitro* transcription using a mMESSAGE mMACHINE T7 ULTRA Kit (Life Technologies, Carlsbad, CA, USA), following the manufacturer's instructions. To generate a *Kdm4b* DNA template for *in vitro* transcription, pCMV-SPORT6 containing the full-length *Kdm4b* mRNA was used as the PCR template (DNAFORM, Kanagawa, Japan, Clone ID 3490671). *Egfp* cDNA was cloned using the pGEM-T Easy Vector System (Promega, Madison, WI, USA) and transcribed *in vitro* using the mMESSAGE mMACHINE T7 ULTRA Kit (Life Technologies) following the manufacturer's instructions. The concentrations of the mRNAs were adjusted to 150 ng ml^{-1} (*Egfp*), 550 ng ml^{-1} (*Kdm3a*), or 450 ng ml^{-1} (*Kdm4b*) to maintain a constant number of injected mRNA molecules. The primer sequences used for generating the templates for *in vitro* transcription are shown in Supplementary Table 9.

***Rnf12* knockdown.** siRNA targeting *Rnf12* (si-Rnf12 sense 5′-GAAGUCAAAUG GAUCGCUUTT-3′ A and antisense 5′-AAAGCGAUCCAUUUGACUUCTG-3′ GC, and the negative control siRNA (si-control: 4390846) were purchased from Life Technologies. The final concentration of each siRNA was 50 ng ml^{-1}. The siRNA was injected into MII oocytes using the Piezo drive and then incubated for 6–7 h in KSOM medium at 37 °C in an atmosphere containing 5% CO_2 before mRNA injection. For the NT experiment using *Rnf12*-knockdown oocytes, oocytes were incubated for 5–6 h after siRNA injection, and NT was then conducted and activated as described above.

Immunofluorescence. Oocytes injected with mRNAs were subjected to ICSI. After 10–11 h, the zygotes were fixed with 2% paraformaldehyde (PFA) in PBS containing 0.1% polyvinyl alcohol (PBS-PVA) for 15 min at room temperature (RT). Zygotes were then permeabilized using 0.2% Triton X-100 in PBS-PVA for 15 min at RT and blocked in 1% BSA in PBS-PVA for 1 h at RT. The primary antibodies used in the assay were as follows: anti-H3K9me3 (ab8898, 1:500 dilution, Abcam, Cambridge, UK), anti-H3K9me2 (ab1220, 1:500, Abcam) and anti-H3K27me3

(07-449, 1:150, EMD Millipore). The primary antibodies were diluted with blocking solution (PBS-PVA containing 1% BSA) and the embryos were incubated overnight at 4 °C. After washing in blocking solution, the embryos were incubated for 1 h at RT with Alexa Flour 634- or 546-conjugated anti-mouse or anti-rabbit IgG secondary antibodies (1:500, Life Technologies). After the embryos were washed, the nuclei were stained with 1 μg ml^{-1} 4′,6-diamidino-2-phenylindole and the embryos were placed on a glass slide and observed with a LSM510 laser scanning confocal microscope (Carl Zeiss, Oberkochen, Germany). Signal intensities of maternal and paternal pronuclei were calculated using NIH ImageJ software (http://rsb.info.nih.gov/ij/).

In *Rnf12*-knockdown experiments, one-cell and four-cell PEs were fixed at 10–11 h (18–19 h after siRNA injection) and 48 h after activation, respectively. Anti-RNF12 (1:500, Abnova, Taipei, Taiwan) and Alexa Fluor 488-conjugated anti-mouse IgG antibodies (1:500, Life Technologies) were used as the primary and secondary antibodies, respectively. *Rnf12*-knockdown and negative-control PEs were observed under the same conditions, to assess knockdown efficiency. Signal intensities were calculated using ImageJ software.

Fluorescent *in situ* hybridization. The zona pellucida of embryos was removed using acid Tyrode solution (Sigma-Aldrich) and then fixed and permeabilized with 2% PFA-PVA containing 0.25% Triton X-100 for 10 min on ice. The samples were placed on glass slides, evaporated to dryness, dehydrated sequentially in 70 and 100% ethanol and then air-dried. Hybridization buffer containing an *Xist* probe (provided by T. Sado) was prepared using a Nick Translation Kit (Abbott, Abbott Park, IL, USA) and Cy3-dUTP (GE Healthcare Life Sciences, Fairfield, CT, USA) and was then applied to the slides. The slides were then incubated and washed as previously described[26]. Fluorescence was visualized using the LSM510.

IF combined with FISH. The zona pellucida of embryos was removed using acid Tyrode solution (Sigma-Aldrich) and fixed with 2% PFA-PVA for 15 min at RT in four-well dishes. The fixed samples were permeabilized with 0.5% Triton X-100 in PBS-PVA for 20 min on ice. After washing with PBS-PVA, the samples were blocked in 1% BSA-PBS-PVA containing 1.3 U ml^{-1} RNaseOUT (Life Technologies) for 30 min at RT. After washing, the embryos were incubated with primary antibodies (anti-CDX2 (BioGenex, San Ramon, CA, USA), diluted 1:30 and anti-H3K27me3 diluted 1:150 in blocking buffer containing 1.3 U ml^{-1} RNaseOUT) for 1 h at RT. Secondary antibody reactions were performed as described above. The samples were placed on glass slides, evaporated to dryness, dehydrated sequentially in 70 and 100% ethanol and air dried. The samples were then analysed by FISH according to the procedures described above.

Analysis of IF combined with FISH data. *Xist* cloud signals detected in three-dimensional images using *Z*-sections of the LSM Image Browser (Carl Zeiss) were judged as positive. Only cells that did not overlap at interphase were used in the analysis. Biallelic expression was defined as cells with two *Xist* cloud spots. Statistical analysis was performed using Fisher's exact test.

Gene expression analysis. Total RNA was extracted using an RNeasy Micro Kit (Qiagen, Venlo, The Netherlands) and treated with DNase following the manufacturer's instructions. mRNAs were reverse transcribed using an oligo(dT) primer and SuperScriptIII Reverse Transcriptase (Life Technologies). For quantitative gene expression analysis with high specificity, TaqMan probes (Life Technologies) were used in all assays. In four-cell stage embryos, *Xist* was assayed in triplicate and only the samples that were detected in two or three replicates were judged as positive. In morulae and blastocysts, expression of target genes was assayed in duplicate. *Gapdh* was used as the internal control in the four-cell-stage assays and *Rnf12* was used in the time-lapse assays. *Gapdh* and *Actb* (encoding β-actin) were used as internal controls at the morula and blastocyst stages. For normalization of qPCR analysis (Fig. 2b,g), the expression levels of all embryos were normalized to the average expression levels of *Egfp*-PEs. The TaqMan probes and primer sets used in this study are shown in Supplementary Table 8.

Generation of *Kdm4b*-inducible ES cell lines and ES cell culture. The XhoI- and ClaI-linearized pGEM-IRES-EGFP plasmids were inserted into the cognate sites of pPB-CAG-EBNX (provided by A. Bradley) to generate pPB-CAG-IRES-EGFP. A Tet3G fragment with BglII and XhoI cleavage sites was amplified from a pEF1a-Tet3G template (Clontech Laboratories, Mountain View, CA, USA) using PCR and inserted into pPB-CAG-IRES-EGFP, generating the vector pPB-CAG-Tet3G-IRES-EGFP. The XhoI and BamHI cleavage sites in pPB-UbC (provided by A. Bradley) were replaced with the p-TRE3G multiple cloning sites (Clontech). The *Kdm4b* coding sequence, with terminal ClaI and BamHI cleavage sites, was amplified by PCR and inserted into the corresponding sites of pPB-TRE3G, yielding pPB-TRE-Kdm4b.

The NCH.4.6 male mouse ES cell line (C57B6/N × C57B6/N), which had a normal karyotype, was electroporated with pPB-TRE-Kdm4b, pPB-CAG-Tet3G-IRES-EGFP and pCMV-hyPBase (provided by A. Bradley). All ES cells used in this study were cultured in knockout DMEM (Life Technologies) containing recombinant human leukemia inhibitory factor culture supernatant for mouse ES cell culture (Wako Pure Chemical Industries, Ltd, Osaka, Japan), as well as GlutaMAX, 2-mercaptoethanol, non-essential amino acids and 15% KSR (all from Life Technologies). Doxycycline (2 μg ml^{-1}; Sigma-Aldrich) was added to ES cell culture medium to induce ectopic KDM4B expression.

Western blotting. Cells were extracted using a stock lysis buffer containing 1 M Tris–HCl, 5 M NaCl, 10% Triton-X and protease inhibitors, and were subjected to e-PAGEL (ATTO, Amherst, NY, USA) electrophoresis. The membranes were washed in TBS containing 0.1% Tween 20 (TBS-T) and blocked in 5% skim milk in TBS-T for 1 h. The membranes were incubated with anti-KDM4B antibodies (1:500 dilution; Active Motif, Carlsbad, CA, USA) overnight at 4 °C, washed and incubated with a rabbit horseradish peroxidase-conjugated secondary antibody (1:5,000 dilution; Sigma-Aldrich) for 1 h at RT. Immunoblottings were visualized using SuperSignal chemiluminescent substrate (Thermo Scientific, Waltham, MA, USA) and an ImageQuant LAS4000 system (GE Healthcare). After capturing the images, the membranes were washed with WB Stripping Buffer (Nacalai Tesque, Kyoto, Japan) for 10 min, washed with TBS-T and incubated with an anti-β-actin antibody conjugated to fluorescein isothiocyanate (1:2,000 dilution; Sigma-Aldrich) for 1 h at RT.

ChIP analysis of K4B-ES cells. Trypsinized feeder-free ES cells (2×10^7) were collected and fixed with 1% formaldehyde. The cells were resuspended in SDS lysis buffer (ChIP Reagent, Nippon Gene Co., Ltd.) and the lysate was sonicated to fragment chromatin using a S220 Focused-ultrasonicator (Covaris, Woburn, MA, USA). The chromatin was purified by centrifugation and immunoprecipitated with Protein A-beads (Veritas Life Sciences, Ribeirão Preto, Brazil) conjugated to anti-H3K9me3 antibodies (Abcam: ab8898) or rabbit IgG (Abcam: ab37415) in Buffer A with protease inhibitor (LowCell ChIP kit, Diagenode, Denville, NJ, USA) overnight at 4 °C. The chromatin beads were washed with Buffers A and C (LowCell ChIP kit). After washing, the chromatin beads were incubated in ChIP direct elution buffer (ChIP Reagent) for 6 h at 65 °C, following incubation with 2 μl proteinase K (20 mg0 ml^{-1}) for 2 h at 55 °C. The DNA immunoprecipitated from the supernatant was purified using Agencourt AMPure XP beads (Beckman Coulter, Inc., Pasadena, CA, USA) according to the manufacturer's instructions.

ChIP combined with deep sequencing. ChIP-Seq libraries were prepared using the NEBNext ChIP-Seq Library Prep Master Mix Set and Multiplex Oligos from Illumina (New England BioLabs Inc., Ipswich, MA, USA) according to the manufacturer's instructions. Ten nanograms of ChIP or input DNA was subjected to end repair, dA-tailing and adaptor ligation, and amplified using nine cycles of PCR. The final library size was checked using a 2100 Bioanalyzer (Agilent Technologies, Santa Clara, CA, USA). After the concentration of each library was determined using qPCR with a KAPA Library Quantification Kit-Illumina/Universal system (KK4824, Kapa Biosystems, Wilmington, MA, USA), the libraries were sequenced using the HiSeq 1000 sequencing system (Illumina, San Diego, CA, USA) to generate 100 bp × 2 paired-end data.

ChIP-seq data analysis. Reads from each sample were first trimmed by removing adapter sequences and low-quality bases at ends using Trimmomatic 0.22 (http://www.usadellab.org/cms/index.php?page=trimmomatic). Approximately 115 million reads for each of the ChIP and input libraries were aligned to the mouse reference genome (mm10:http://genome.ucsc.edu/cgi-bin/hgGateway) using the Burrows-Wheeler Aligner 0.6.2. Uniquely mapped reads were selected using a custom script, converted from SAM to BAM format using SAMtools 0.1.18 and processed using Picard 1.83 to mark PCR duplicates. Reads with a mapping quality of <20 were removed using SAMtools 0.1.18. The resulting BAM files (a pair of files for ChIP and input libraries) were visualized using the Integrative Genomics Viewer (http://www.broadinstitute.org/igv/) and subjected to peak detection using the MACS algorithm implemented in Avadis NGS software (Agilent). In scatter plot analysis using 1 and 15 K4B-ES cell lines, the numbers of mapped reads were counted for 10,000-bp windows (with a sliding size of 5,000 bp). To adjust for differences in total amount of reads, the number of mapped reads in each window was transformed into reads per million format. Calculation methods are available on request.

ChIP-qPCR analysis of sperm. Sperm were obtained from BDF1 mice aged 9–12 weeks. Preparation of sperm chromatin was performed according to published protocols with modifications[39,40]. For each native ChIP experiment, 5×10^7 sperm were used. Sperm were washed twice with PBS. The pellet was suspended in PBS containing 0.5% Triton-X, 10 mM dithiothreitol (DTT) and protease inhibitor (Diagenode), and incubated on ice for 1.5 h. After washing with PBS, pelleted sperm nuclei were suspended in 400 μl PBS containing 1 mM $CaCl_2$ and 1 mM DTT, and incubated for 5 min at 37 °C. After incubation, 1 μl (2×10^6 gel units per ml) micrococcal nuclease (New England BioLabs) was added to the nuclei, which were then incubated for 5 min at 37 °C. EDTA was added to a concentration of 0.5 mM and solubilized chromatin was clarified by centrifugation for 15 min at 15,000 r.p.m. at 4 °C. The pellets were suspended in PBS containing $CaCl_2$ and DTT (at the same concentrations as used above), and treated again with micrococcal nuclease. To examine whether H3K9me3-modified nucleosomes were

present in sperm chromatin, soluble (chromatin) and insoluble (pellet) fractions were subjected to western blotting using anti-H3K9me3 antibodies (ab8898; 1:1,000), as described above.

Chromatin was incubated with Protein A beads conjugated to anti-H3K9me3 antibodies (ab8898) or rabbit IgG (ab37415) overnight at 4 °C in ChIP buffer (40 mM Tris–HCl, pH 7.5, 1 M NaCl and 10 mM EDTA). Pelleted beads were washed twice with Buffer 1 (50 mM Tris–HCl, pH 7.5, 500 mM NaCl and 10 mM EDTA) and Buffer 2 (50 mM Tris-HCL, pH 7.5, 300 mM NaCl and 10 mM EDTA). The pelleted beads were suspended in ChIP direct elution buffer and incubated with proteinase K for 2 h at 37 °C. The immunoprecipitated DNA was then purified using Agencourt AMpure XP beads.

ChIP-qPCR analysis was performed according to published methods using SYBR Green[39]. The sequences of each primer set are listed in Supplementary Table 9.

eChIP-quantitative qPCR. The zona pellucidae of the embryos were removed by acid Tyrode's solution and washed in PBS containing 0.1% PVA. The embryos were suspended in PBS containing 0.5% Triton-X, 0.5 mM DTT and protease inhibitor, and incubated on ice for 30 min. After incubation, 1 mM $CaCl_2$ was added to the buffer and samples were incubated for 5 min at 37 °C. After incubation, 0.5 μl (2×10^6 gel units per ml) micrococcal nuclease (New England BioLabs) was added to the nuclei, which were then incubated for 5 min at 37 °C. EDTA was added to a concentration of 0.5 mM and solubilized chromatin was clarified by centrifugation at 15,000 r.p.m. for 15 min at 4 °C. The same procedures were repeated one more time. Chromatin was incubated with Protein A beads conjugated to anti-H3K9me3 antibodies (ab8898) or rabbit IgG (ab37415), prepared as described above, overnight at 4 °C in ChIP buffer (40 mM Tris–HCL, pH 7.5, 1 M NaCl and 10 mM EDTA). Pelleted beads were washed twice with Buffer 1 (50 mM Tris–HCL, pH 7.5, 500 mM NaCl and 10 mM EDTA) and then with Buffer 2 (50 mM Tris–HCL, pH 7.5, 300 mM NaCl and 10 mM EDTA). The pelleted beads were then suspended in ChIP direct elution buffer and incubated with proteinase K for 2 h at 55 °C. The immunoprecipitated DNA was then purified using Agencourt AMpure XP beads.

Eluted DNA (20 μl) was divided into two aliquots; one (4 μl) was used for a SYBR Green assay targeting a major satellite and the other (16 μl) was subjected to pre-amplification using a Single Cell-to-CT kit (Ambion, Austin, TX, USA) according to the manufacturer's instructions. The number of PCR cycles at the pre-amplification step was 20. The primer and probe sequences used are shown in Supplementary Table 9.

Microarray analysis. Five *Egfp*-PE, *Kdm4b*-PE and IVF blastocysts (120 h) were lysed using ISOGEN (Nippongene) and RNA was extracted by phenol–chloroform and isopropanol precipitation. cDNA was synthesized using the Ovation RNA Amplification System V2 kit (NuGEN, West Cumbria, UK) and hybridized with SurePrint G3 Mouse GE 8x60K Microarray (Agilent Technologies). Analysis was conducted using GeneSpringV12.5 (Agilent Technologies). Transcripts were considered to be expressed if raw values were >100 and a flag was present in at least one of the groups.

References

1. Augui, S., Nora, E. P. & Heard, E. Regulation of X-chromosome inactivation by the X-inactivation centre. *Nat. Rev. Genet.* **12,** 429–442 (2011).
2. Lee, J. T. Gracefully ageing at 50, X-chromosome inactivation becomes a paradigm for RNA and chromatin control. *Nat. Rev. Mol. Cell Biol.* **12,** 815–826 (2011).
3. Wutz, A. Gene silencing in X-chromosome inactivation: advances in understanding facultative heterochromatin formation. *Nat. Rev. Genet.* **12,** 542–553 (2011).
4. Takagi, N. & Sasaki, M. Preferential inactivation of the paternally derived X chromosome in the extraembryonic membranes of the mouse. *Nature* **256,** 640–642 (1975).
5. Shin, J. *et al.* Maternal Rnf12/RLIM is required for imprinted X-chromosome inactivation in mice. *Nature* **467,** 977–981 (2010).
6. Tada, T. *et al.* Imprint switching for non-random X-chromosome inactivation during mouse oocyte growth. *Development* **127,** 3101–3105 (2000).
7. Chiba, H. *et al. De novo* DNA methylation independent establishment of maternal imprint on X chromosome in mouse oocytes. *Genesis* **46,** 768–774 (2008).
8. Marahrens, Y., Panning, B., Dausman, J., Strauss, W. & Jaenisch, R. Xist-deficient mice are defective in dosage compensation but not spermatogenesis. *Genes Dev.* **11,** 156–166 (1997).
9. Liu, N. *et al.* Genome-wide gene expression profiling reveals aberrant MAPK and Wnt signaling pathways associated with early parthenogenesis. *J. Mol. Cell Biol.* **2,** 333–344 (2010).
10. Obata, Y. & Kono, T. Maternal primary imprinting is established at a specific time for each gene throughout oocyte growth. *J. Biol. Chem.* **277,** 5285–5289 (2002).
11. Kono, T. *et al.* Birth of parthenogenetic mice that can develop to adulthood. *Nature* **428,** 860–864 (2004).
12. Kawahara, M. *et al.* High-frequency generation of viable mice from engineered bi-maternal embryos. *Nat. Biotechnol.* **25,** 1045–1050 (2007).
13. Santos, F., Peters, A. H., Otte, A. P., Reik, W. & Dean, W. Dynamic chromatin modifications characterise the first cell cycle in mouse embryos. *Dev. Biol.* **280,** 225–236 (2005).
14. Cantone, I. & Fisher, A. G. Epigenetic programming and reprogramming during development. *Nat. Struct. Mol. Biol.* **20,** 282–289 (2013).
15. Lewis, A. *et al.* Imprinting on distal chromosome 7 in the placenta involves repressive histone methylation independent of DNA methylation. *Nat. Genet.* **36,** 1291–1295 (2004).
16. Yuan, P. *et al.* Eset partners with Oct4 to restrict extraembryonic trophoblast lineage potential in embryonic stem cells. *Genes Dev.* **23,** 2507–2520 (2009).
17. Fodor, B. D. *et al.* Jmjd2b antagonizes H3K9 trimethylation at pericentric heterochromatin in mammalian cells. *Genes Dev.* **20,** 1557–1562 (2006).
18. Nakamura, T. *et al.* PGC7 binds histone H3K9me2 to protect against conversion of 5mC to 5hmC in early embryos. *Nature* **486,** 415–419 (2012).
19. Nesterova, T. B., Barton, S. C., Surani, M. A. & Brockdorff, N. Loss of Xist imprinting in diploid parthenogenetic preimplantation embryos. *Dev. Biol.* **235,** 343–350 (2001).
20. Plath, K. *et al.* Role of histone H3 lysine 27 methylation in X inactivation. *Science* **300,** 131–135 (2003).
21. Okamoto, I., Tan, S. & Takagi, N. X-chromosome inactivation in XX androgenetic mouse embryos surviving implantation. *Development* **127,** 4137–4145 (2000).
22. Barakat, T. S. *et al.* RNF12 activates Xist and is essential for X chromosome inactivation. *PLoS Genet.* **7,** e1002001 (2011).
23. Puschendorf, M. *et al.* PRC1 and Suv39h specify parental asymmetry at constitutive heterochromatin in early mouse embryos. *Nat. Genet.* **40,** 411–420 (2008).
24. Dahl, J. A. & Collas, P. A rapid micro chromatin immunoprecipitation assay (microChIP). *Nat. Protoc.* **3,** 1032–1045 (2008).
25. Turner, B. in *Mapping Protein/DNA Interactions by Cross-Linking* (2001).
26. Hoki, Y. *et al.* A proximal conserved repeat in the Xist gene is essential as a genomic element for X-inactivation in mouse. *Development* **136,** 139–146 (2009).
27. Fukuda, A. *et al.* Identification of inappropriately reprogrammed genes by large-scale transcriptome analysis of individual cloned mouse blastocysts. *PLoS ONE* **5,** e11274 (2010).
28. Inoue, K. *et al.* Impeding Xist expression from the active X chromosome improves mouse somatic cell nuclear transfer. *Science* **330,** 496–499 (2010).
29. Marks, H. *et al.* The transcriptional and epigenomic foundations of ground state pluripotency. *Cell* **149,** 590–604 (2012).
30. Karimi, M. M. *et al.* DNA methylation and SETDB1/H3K9me3 regulate predominantly distinct sets of genes, retroelements, and chimeric transcripts in mESCs. *Cell Stem Cell* **8,** 676–687 (2011).
31. Ono, Y. & Kono, T. Irreversible barrier to the reprogramming of donor cells in cloning with mouse embryos and embryonic stem cells. *Biol. Reprod.* **75,** 210–216 (2006).
32. Dindot, S. V., Person, R., Strivens, M., Garcia, R. & Beaudet, A. L. Epigenetic profiling at mouse imprinted gene clusters reveals novel epigenetic and genetic features at differentially methylated regions. *Genome Res.* **19,** 1374–1383 (2009).
33. Sasaki, H. & Matsui, Y. Epigenetic events in mammalian germ-cell development: reprogramming and beyond. *Nat. Rev. Genet.* **9,** 129–140 (2008).
34. Sugimoto, M. & Abe, K. X chromosome reactivation initiates in nascent primordial germ cells in mice. *PLoS Genet.* **3,** e116 (2007).
35. Duszczyk, M. M., Wutz, A., Rybin, V. & Sattler, M. The Xist RNA A-repeat comprises a novel AUCG tetraloop fold and a platform for multimerization. *RNA* **17,** 1973–1982 (2011).
36. Gontan, C. *et al.* RNF12 initiates X-chromosome inactivation by targeting REX1 for degradation. *Nature* **485,** 386–390 (2012).
37. Zhang, L. *et al.* RNF12 controls embryonic stem cell fate and morphogenesis in zebrafish embryos by targeting Smad7 for degradation. *Mol. Cell* **46,** 650–661 (2012).
38. Shin, J. *et al.* RLIM is dispensable for X-chromosome inactivation in the mouse embryonic epiblast. *Nature* **511,** 86–89 (2014).
39. Brykczynska, U. *et al.* Repressive and active histone methylation mark distinct promoters in human and mouse spermatozoa. *Nat. Struct. Mol. Biol.* **17,** 679–687 (2010).
40. Hammoud, S. S. *et al.* Distinctive chromatin in human sperm packages genes for embryo development. *Nature* **460,** 473–478 (2009).

Acknowledgements

We are grateful to T. Sado for critical reading of this manuscript and discussions. We thank T. Sugawara and H. Kobayashi for helpful comments; A. Bradley for providing the PiggyBac vector; K. Kusakabe, T. Kikuchi, Y. Harada, S. Kanai and Y. Takahashi for technical assistance with some experiments and analysis; and T. Kawasaki for preparation of figures. This work was supported by grants from the Ministry of Education, Culture, Sports, Science and Technology (MEXT) of Japan; a grant from the Ministry of Health, Labour and Welfare (MHLW) to H.A. and A.U.; a Grant-in-aid for Scientific

Research (21390456); a grant from JST-CREST to H.A.; and a JSPS KAKENHI Grant-in-Aid for Research Activity Start-up to A.F. (24890300).

Author contributions

A.F., K.E. and H.A. conceived and designed the study. A.F. performed the experiments and analysis of embryo manipulation, IF, FISH, qPCR, ChIP, cultured ES cells, vector construction and microarray analysis, and developed the eChIP-qPCR technique. J.T., K.H. and K.N. conducted ChIP-seq experiments and analyses. T.M. and H.A. constructed vectors and cultured ES cells. H.A. and A.U. supervised the study. A.F., K.N. and H.A. wrote the manuscript.

Additional information

Accession codes: The original data for the microarray have been deposited in the GEO at http://www.ncbi.nlm.nih.gov/geo/ (accession number: GSE53662). The original data of ChIP-seq have been deposited in DDBJ at http://cibex.nig.ac.jp/index.jsp with accession number: DRA001041.

Supplementary Information accompanies this paper at http://www.nature.com/naturecommunications

Competing financial interests: The authors declare no competing financial interests.

Reprints and permission information is available online at http://npg.nature.com/reprintsandpermissions/

How to cite this article: Fukuda, A. *et al.* The role of maternal-specific H3K9me3 modification in establishing imprinted X-chromosome inactivation and embryogenesis in mice. *Nat. Commun.* 5:5464 doi: 10.1038/ncomms6464 (2014).

Induced cancer stem-like cells as a model for biological screening and discovery of agents targeting phenotypic traits of cancer stem cell

Mayuko Nishi[1], Hidenori Akutsu[2], Ayumi Kudoh[1], Hirokazu Kimura[3], Naoki Yamamoto[4], Akihiro Umezawa[2], Sam W. Lee[5] and Akihide Ryo[1]

[1] Department of Microbiology, Yokohama City University School of Medicine, Yokohama, Japan

[2] Department of Reproductive Biology, National Research Institute for Child Health and Development, Tokyo, Japan

[3] Infectious Disease Surveillance Center, National Institute of Infectious Diseases, Tokyo, Japan

[4] Department of Microbiology, National University of Singapore, Singapore

[5] Cutaneous Biology Research Center, Massachusetts General Hospital and Harvard Medical School, Charlestown, MA, USA

Correspondence to: *Akihide Ryo,* ***email:*** *aryo@yokohama-cu.ac.jp*

Keywords: Cancer stem cell, p21Cip1, drug screening, senescence, tumor sphere formation

Received: *June 07, 2014* ***Accepted:*** *August 16, 2014* ***Published:*** *August 17, 2014*

ABSTRACT

Cancer stem cells (CSCs) retain the capacity to propagate themselves through self-renewal and to produce heterogeneous lineages of cancer cells constituting the tumor. Novel drugs that target CSCs can potentially eliminate the tumor initiating cell population therefore resulting in complete cure of the cancer. We recently established a CSC-like model using induced pluripotent stem cell (iPSC) technology to reprogram and partially differentiate human mammary epithelial MCF-10A cells. Using the induced CSC-like (iCSCL) model, we developed a phenotypic drug assay system to identify agents that inhibit the stemness and self-renewal properties of CSCs. The selectivity of the agents was assessed using three distinct assays characterized by cell viability, cellular stemness and tumor sphere formation. Using this approach, we found that withaferin A (WA), an Ayurvedic medicine constituent, was a potent inhibitor of CSC stemness leading to cellular senescence primarily via the induction of $p21^{Cip1}$ expression. Moreover, WA exhibited strong anti-tumorigenic activity against the iCSCL. These results indicate that our iCSCL model provides an innovative high throughput platform for a simple, easy, and cost-effective method to search for novel CSC-targeting drugs. Furthermore, our current study identified WA as a putative drug candidate for abrogating the stemness and tumor initiating ability of CSCs.

INTRODUCTION

Cancer stem cells (CSCs) are defined as transformed stem cells that possess characteristics associated with normal stem cells, specifically the ability to self-renew and to form hierarchical cancer tissues [1]. Accumulating evidence has shown that CSCs reside in various solid tumors where they function as a sub-population that plays a critical role in tumor initiation, progression, metastasis, and recurrence [2, 3]. Therefore, CSCs are considered to be a source of the tumor initiation and dissemination as well as the acquisition of malignant properties [4]. CSCs are commonly resistant to conventional anti-cancer treatments such as chemotherapeutic agents and radiation therapy resulting in treatment failure [5, 6]. In order to overcome this treatment limitation, novel therapeutic strategies should aim to eliminate CSCs which should effectively eradicate the cancer initiating cell population within tumor tissues [7].

The development of new treatment strategies that target CSCs is one of the main goals of anti-cancer therapy. However, in general, a large-scale drug screening process requires a large supply of stable and homogeneous cells to ensure reproducibility of the assay [8]. It is necessary to separate a sufficient number of CSCs from tumor tissue, to amplify the CSCs while stably

maintaining them in an undifferentiated state *in vitro*. To date, the optimal cell culture conditions for amplifying pure CSC populations remain undefined. In fact, *in vitro* amplified CSCs are largely incompatible with the *in vivo* tumor microenvironment resulting in cell death or dormancy [9]. Moreover, cellular heterogeneity of bulk of CSC populations may reduce the fidelity and feasibility of drug screening assays [10]. Recently, several research groups attempted to establish new human CSC models [11, 12]. Currently, separation and purification of cancer stem-like cells from some cancer cell lines is the most common and easy method. Cancer stem-like cells can be enriched by collecting cells expressing CSC markers such as CD133 and CD44 [13, 14]. ALDEFLUOR™ is a non-immunological method that identifies human stem/progenitor cells based on their aldehyde dehydrogenase (ALDH) activity [15]. Interestingly, co-expression of $CD133^+$ and $CD44^+$ with high ALDH activity identified an enriched CSC-like population within established cancer cell lines [16]. An alternative approach for the enrichment of CSCs is the use of transformed cancer cell lines that were forced to undergo the tumor sphere formation or the epithelial-to-mesenchymal transition (EMT) [17, 18]. These cells expressed surrogate CSC markers and displayed putative tumorigenic properties *in vivo*, which highlights the potential suitability of this model for the discovery of compounds that can selectively target CSCs [19]. Despite the advances in modeling CSCs, the genetic variability with chromosomal instabilities in over-passaged cell lines remains a limitation that prevents consistent findings in large-scale drug screening assay. Furthermore, tumor sphere culture cannot always enrich cancer stem-like cells from cancer cell lines [20].

To overcome the aforementioned caveats, we recently developed a novel method of inducing cancer stem-like cells through the reprogramming and partial differentiation of the immortalized human mammary epithelial MCF-10A cell line which has a low genetic mutation rate [21]. These cells, termed induced cancer stem cell-like 10A (iCSCL-10A), express cancer stem markers (CD44, CD133 and ALDH1) and show much higher sphere forming ability than conventional cancer cell lines even in regular cell culture media supplemented with fetal bovine serum [22]. Furthermore, only several hundreds of iCSCL-10A cells can form hierarchically-organized tumors in immunosuppressed mice in a short period [22]. In our current study, we utilized iCSCL-10A cells to identify agents that selectively prohibit the traits of CSCs. Rather than simply identifying drugs that kill CSCs, we sought to identify compounds that interfere with the self-renewal and pluripotent properties of CSCs [23]. We found that Withaferin A (WA) was a putative anti-CSC drug candidate that altered the tumorigenic properties of CSC via the induction of cellular senescence. Our current approach can thus provide an useful option for future development of anti-CSC drugs.

RESULTS

Development of a drug screening assay system based on CSC properties

We recently established a new CSC-like model, iCSCL-10A cells, via the introduction of defined reprogramming factors and subsequent partial cell differentiation from MCF-10A cells [22, 24]. These proliferating CSC-like cells express characteristic CSC markers, display a malignant phenotype *in vitro* and form tumors of multiple lineages following injection into immunocompromised mice (Figure 1A) [25]. We utilized iCSCL-10A cells for our high-throughput drug screening assay to monitor phenotypic traits of CSCs in the presence of various compounds. We aimed to identify compounds that selectively target CSCs by monitoring the specific properties of CSC, such as self-renewal and stemness, without prominent cell toxicity. The activity/selectivity of the agents was assessed using three distinct assays: 1) cell viability assay for cell toxicity, 2) alkaline phosphatase (ALP) assay for cellular stemness, and 3) tumor sphere forming assay for self-renewal. The assays were designed using the 96-well platform for large-scale drug screening (Figure 1B).

Selection of drugs targeting CSC phenotype

As an initial trial, we plated the iCSCL-10A cells in 96-well plates and tested 73 organic compounds using our three assays in parallel (Figure 2A). We used the compounds at relatively lower concentration (1 μM) in order to avoid redundant cytotoxicity. The selective toxicity against CSC-like cells was then determined using the WST-8 assay to monitor cell viability (Figure 2B). Cellular stemness was measured by monitoring expression of the stem cell marker ALP (Figure 2C). Interestingly, we found that a single compound (No. 36) drastically reduced the number of ALP-positive cells with limited cytotoxicity at 1 μM where cell viability was greater than 80%. The compound was identified as Withaferin A (WA) (Figure 2B and C). We next conducted a high-throughput tumor sphere formation assay. We designed a platform of tumor sphere formation for as short as 48 hrs to maximize the rapidity of the assay. We also noticed that WA significantly suppressed tumor sphere formation highlighting its function to abrogate the self-renewal ability of iCSCL-10A cells (Figure 2D). Based on our initial finding, WA was selected for further characterization.

We conducted parallel experiments using varying concentrations of WA. Our results revealed that the stemness of iCSCL-10A cells was abrogated at 0.25 μM of WA as observed using the ALP assay, while the cell viability was inhibited at concentrations greater than

2μM of WA (Figure 3A,B). Tumor sphere formation was inhibited at concentrations as low as 0.125 μM (Figure 3C, D). Collectively, these results indicate that WA could selectively inhibit the stemness of iCSCL-10A cells at relatively low concentrations compared to its impact on cell viability at 10-fold to 15-fold higher concentrations. We hereafter used 1μM WA in our further studies since the effect of WA was prominent at this concentration despite of the minimum cytotoxicity.

WA is the most abundant constituent of Withania somnifera, also known as Ashwagandha, which has been studied extensively for its biologically active constituents, steroidal lactones and withanolides [26]. To further explore the anti-CSC function of WA, we next investigated the activity of three WA compound analogues, Withanone, Withanolide A and 12-Deoxywithastramonolide (12-DWS) (Figure 4A). The parallel experiments for ALP staining and the tumor sphere assays revealed that none of the WA analogues abrogated the stemness and self-renew ability of iCSCL-10A cells (Figure 4B-E), suggesting that the anti-CSC properties were specific to WA.

WA reduces the expression of stem cell and EMT markers

We further examined the effects of WA on the expression of stem cell markers on iCSCL-10A as measure of stemness. It has been well established that the $CD44^{+}$/$CD24^{low}$ fraction identifies the CSC population in solid tumors [13]. WA treatment significantly reduced for this fraction of iCSCL-10A cells (Figure 5A). Reverse transcription polymerase chain reaction (RT-PCR) analysis demonstrated that the expression of stem cell markers, ALDH1A1 and Nanog, were prominently reduced in iCSCL-10A cells treated with WA as compared with DMSO-treated control cells (Figure 5B). Concomitantly, WA reduced the expression of specific stem cell markers

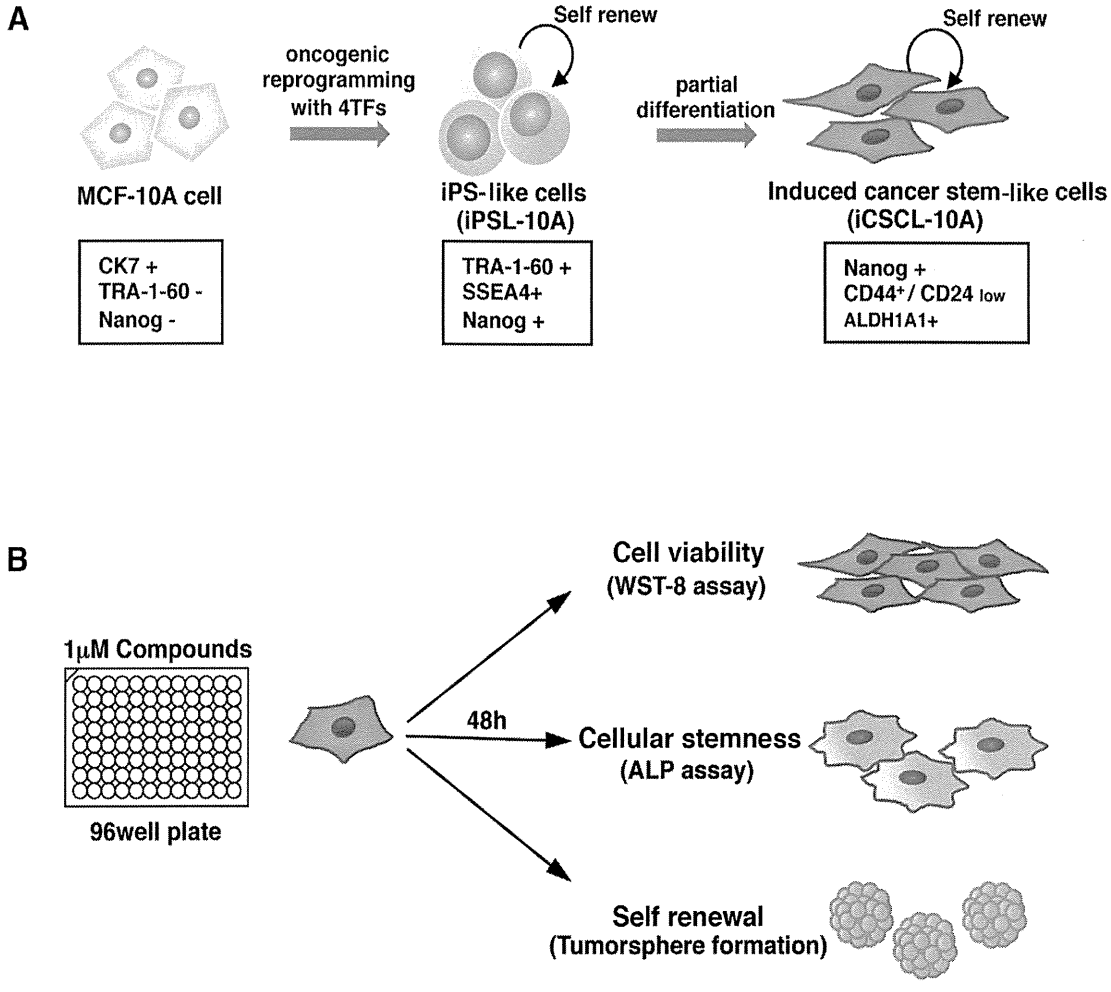

Figure 1: The induced CSC-like model and drug screening method. (A) Non-tumorigenic MCF-10A cells were subjected to oncogenic reprogramming via the transduction of defined reprogramming factors (4TFs) to generate iPS-like cells (iPSL-10A). To generate iCSCL-10A cells with CSC properties, the iPSL-10A cells were then partially differentiated via embryoid body formation. The iPSL-10A cells acquired the ability to form hierarchically organized tumors composed of CSC-like cells and differentiated cells with multiple lineages. (B) Schematic of our drug screening method. To identify compounds with a low cytotoxicity and that abrogated CSC stemness, cell viability, cellular stemness and tumor sphere formation assays were performed in parallel.

A

1	Hyperoside	26	Bilobalide	51	Cryptochlorogenic acid
2	Isoquercitrin	27	Ginkgolide A	52	Neochlorogenic acid
3	Tectoridin	28	Ginkgolide B	53	Isochlorogenic acid A
4	Tectorigenin	29	Ginkgolide C	54	Isochlorogenic acid C
5	6-Hydroxygenistein 6,7-diglucoside	30	Licoricesaponin G2	55	Pedalitin 6-glucoside
6	Tectorigenin 7-o-xylosylglucoside	31	Licoricesaponin H2	56	Simmondsin
7	Daidzin	32	Glycyrrhizinic acid	57	Plantaginin
8	Daidzein	33	Soyasaponin I	58	Calicosin 7-glucoside
9	Glycitin	34	Soyasaponin V	59	Hesperidin
10	Glycitein	35	Withanone	60	PlaeruptorinA
11	Genistin	36	Withaferin A	61	Luteolin 7-glucoside
12	Genistein	37	Pteropodine	62	Quercetin 3-arabinoside
13	Neohesparidin	38	Isopteropodine	63	Rhein
14	Luteolin	39	Mitraphylline	64	Swertiamarin
15	(+)-Catechin	40	Speciophylline	65	Deacyl gimnemic acid
16	(-)-Epicatechin	41	Uncarine F	66	Isorhamnetin-3-O-glucoside
17	(-)-Epigallocatechin	42	Rhynchophylline	67	Isorhamnetin-3-O-rutinoside
18	Quercetin 4'-glucoside	43	Geniposide	68	Quercetin
19	Quercetin 3,4'-diglucoside	44	Arctiin	69	ε-Viniferin
20	rutin dihydrate	45	Chlorogenic acid	70	trans-Resveratrol
21	3,5,7,3',4'-Pentamethoxyflavone	46	Caffeic acid	71	Theogallin
22	5,7,4'-Trimetoxyflavone	47	6-Gingerol	72	Glabridin
23	5,7-Dimethoxyfavone	48	8-Gingerol	73	Riquiritigenin
24	3,5,7-Trimetoxyflavone	49	10-Gingerol		
25	3,5,7,4'-tetramethoxyflavone	50	6-Shogaol		

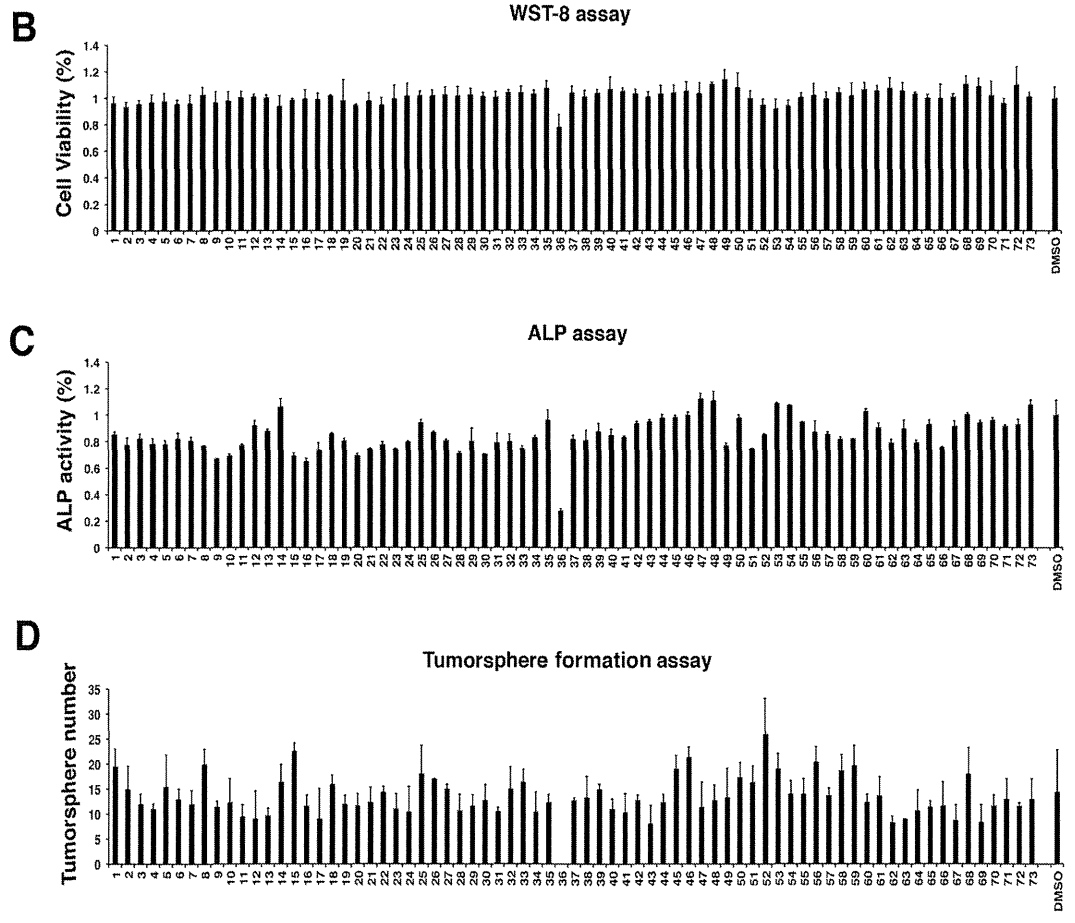

Figure 2: Screening of natural compounds that selectively impede the stemness of iCSCL-10A cells. (A) A list of natural compounds assayed in the study. (B, C) iCSCL-10A cells ($5x10^3$ cells/well in 100 µl) were plated in 96-well plates. After 24 hrs, 1 µM of compound was added to the appropriate wells. Cell viability was measured after 48 hrs using WST-8 (2-(2-methoxy-4-nitrophenyl)-3-(4-nitrophenyl)-5-(2,4-disulfophenyl)-2H-tetrazolium) activity assays (B). Alkaline Phosphatase (ALP) activity was measured after 48 hrs using the TRACP & ALP Assay Kit and a microplate reader. Values represent the mean ± SEM (n = 3) (C). (D) Quantification of tumor sphere formation. iCSCL-10A cells were plated on ultra-low attachment surface 96-well plates in the presence of 1µM of the compounds and tumor sphere formation was assessed at 48 hrs.

SOX2 and Nanog as measured by immunoblotting (Figure 5C). Epithelial-mesenchymal transition (EMT) is closely associated with the properties of CSCs [18]. We then assessed whether WA treatment modulated the expression of EMT regulators. WA treatment downregulated the major EMT markers, Twist and Slug (Figure 5C). Therefore, WA seems to play a dual role in iCSCL-10A cells by suppressing the expression of both stem cell and EMT markers.

WA inhibits cell migration and invasion of iCSCL-10A

A key property of CSCs is its invasive ability. To examine the effect of WA on the invasion of CSCs, we performed a chamber invasion assay using matrigel-coated transwells. We found that WA treatment in iCSCL-10A cells resulted in a markedly reduced capacity for the cells to undergo invasion (Figure 5D).

Another important feature of CSCs is their increased mobility. To evaluate whether WA affects CSC migration in this context, wound-healing assays were performed. WA treatment significantly inhibited the wound healing ability of iCSCL-10A cells (Figure 5E). Therefore, WA treatment profoundly inhibits the tumor invasion and migration properties of CSCs.

WA disrupts the microenvironment of CSC-like spheres

To examine the effect of WA on CSC microenvironment, pre-formed tumor spheres were treated with either WA or DMSO followed by morphological and cell viability analyses (Figure 6A). It was notable that WA significantly reduced the viable cell numbers forming tumor spheres. Concomitantly, tumor spheres exhibited irregular morphology with notched structure around the rims upon WA treatment while no such inhibitory effect was observed in cells treated with DMSO (Figure 6B, C). These results suggest that WA can penetrate into tumor spheres and may disrupt the microenvironment that can be important for the maintenance of CSC stemness.

WA inhibits the tumorigenicity of iCSCL-10A

We subsequently assessed the *in vivo* tumor-forming ability of cells treated with WA. For these

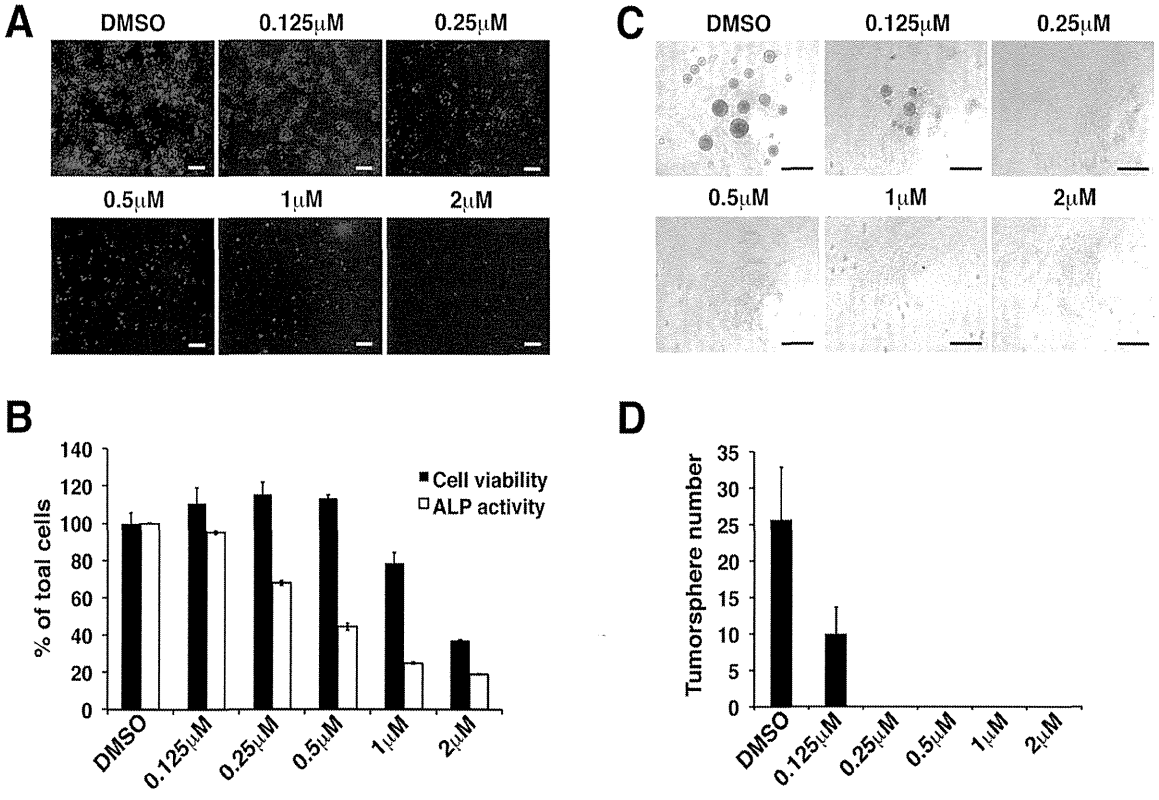

Figure 3: Withaferin A inhibits self-renewal and pluripotent properties of iCSCL-10A cells. (A, B) iCSCL-10A cells were treated with the indicated concentrations of WA and ALP activity was measured after 48 hrs. Phase contrast images of ALP staining in iCSCL-10A cells treated with WA (A). Nuclei were counterstained with 40,6-diamidino-2-phenylindole (DAPI). Scale bar, 500 mm. Cell viability was measured after 48 hrs using WST-8 activity assays. Alkaline Phosphatase (ALP) activity was measured after 48 hrs using the TRACP & ALP Assay Kit and a microplate reader. Values represent the mean ± SEM (n = 3) (B). (C, D) iCSCL-10A cells were plated in the presence of the indicated concentrations of WA and tumor sphere formation was assessed after 48 hrs. Phase contrast images of tumor spheres (C). Values represent the mean ± SEM (n = 3) (D). Scale bar, 500 mm.

experiments, iCSCL-10A cells were treated with varying concentrations of WA *in vitro* for 72 hrs prior to injection into immunosuppressed mice. We observed that iCSCL-10A had a strong tumorigenic property forming tumor mass for only 10 to 12 days as shown in DMSO-treated control cells (Figure 6D). On the other hand, the pre-treatment of WA had a dose-dependent anti-tumor effect on iCSCL-10A cells in both tumor initiation and tumor size (Figure 6D, E).

Next, we assessed the optimal duration for WA pre-treatment for inhibiting tumor formation of CSCs. iCSCL-10A cells were treated with 1.5 μM of WA for varying hours prior to being injected into immunosuppressed mice. WA pre-treatment for more than 24 hrs significantly decreased both the tumor initiation and the tumor-forming ability of iCSCL-10A cells (Figure 6F, G). Taken together, these results indicate that the pre-treatment with WA can abrogate the tumorigenic properties of iCSCL-10A cells.

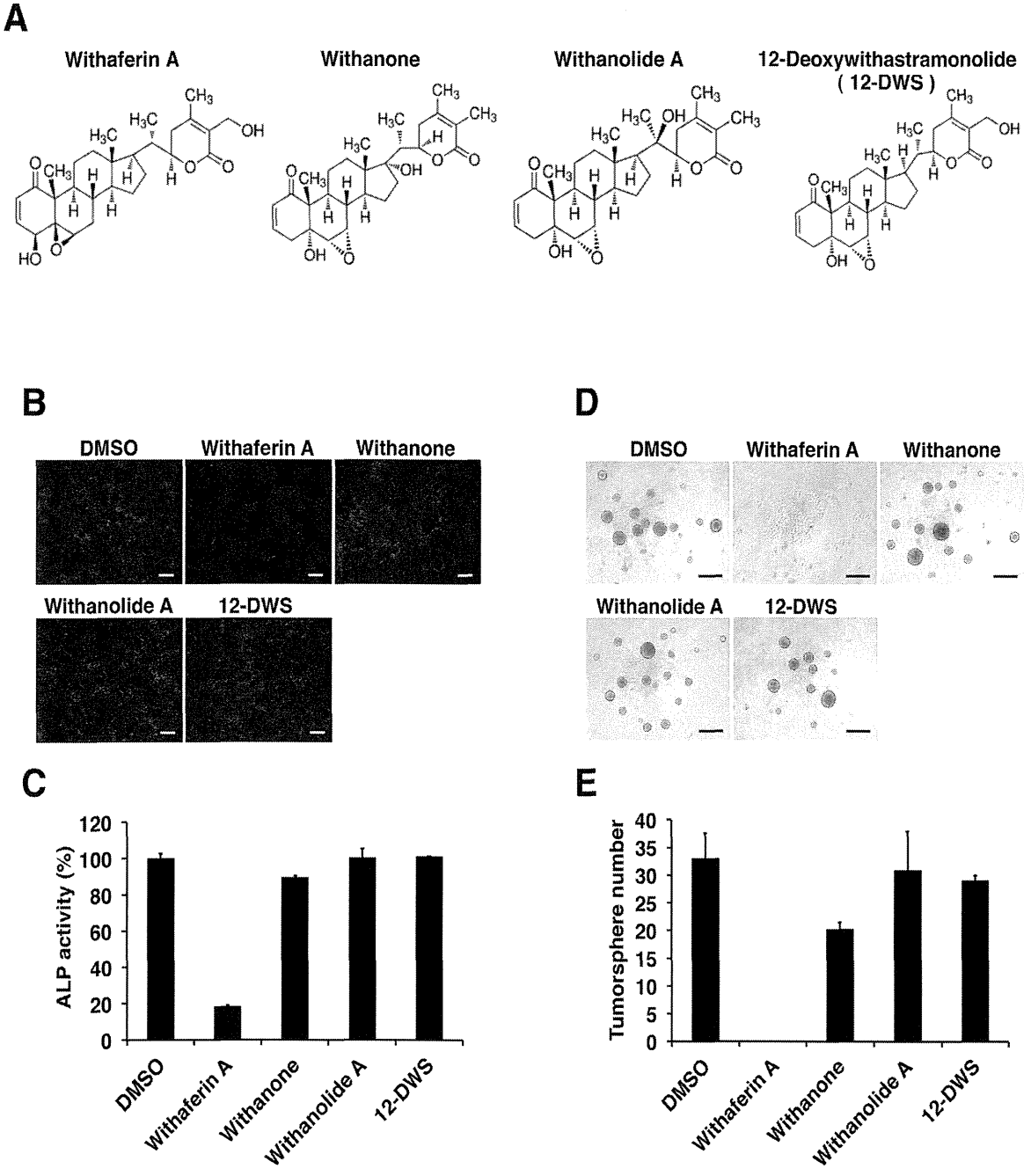

Figure 4: The effect of Withaferin A analogues on the expression of phenotypic CSC properties. (A) Chemical structures of Withaferin A, Withanone, Withanolide A and 12-Deoxywithastramonolide (12-DWS). (B, C) iCSCL-10A cells were treated with 1 μM of Withaferin A, Withanone, Withanolide A, or 12-DWS for 48 hrs followed by the ALP assay. Phase contrast images of ALP staining (B). Values represent the mean ± SEM (n = 3) (C). Scale bar, 500 mm. (D, E) iCSCL-10A cells treated with 1 μM of Withaferin A, Withanone, Withanolide A and 12-DWS for 48 hrs and the tumor spheres were enumerated. Phase contrast images of tumor spheres are shown (D). Scale bar, 500 mm.Values represent the mean ± SEM (n = 3, E).

WA induces the senescence of iCSCL-10A

We next determined the mechanism regulating WA-mediated abrogation of stemness and malignant properties of CSCs. Light microscopy revealed that cell morphology was drastically changed following WA treatment. Cells that were treated with WA were enlarged, flattened and irregular shaped, and they contained increased intracellular granules which were reminiscent of cellular senescence (Figure 7A). These cells were also positively stained with senescence-associated β-galactosidase (SABG) which was not detected in the DMSO-treated cell population (Figure 7A). To further support this observation we tested another

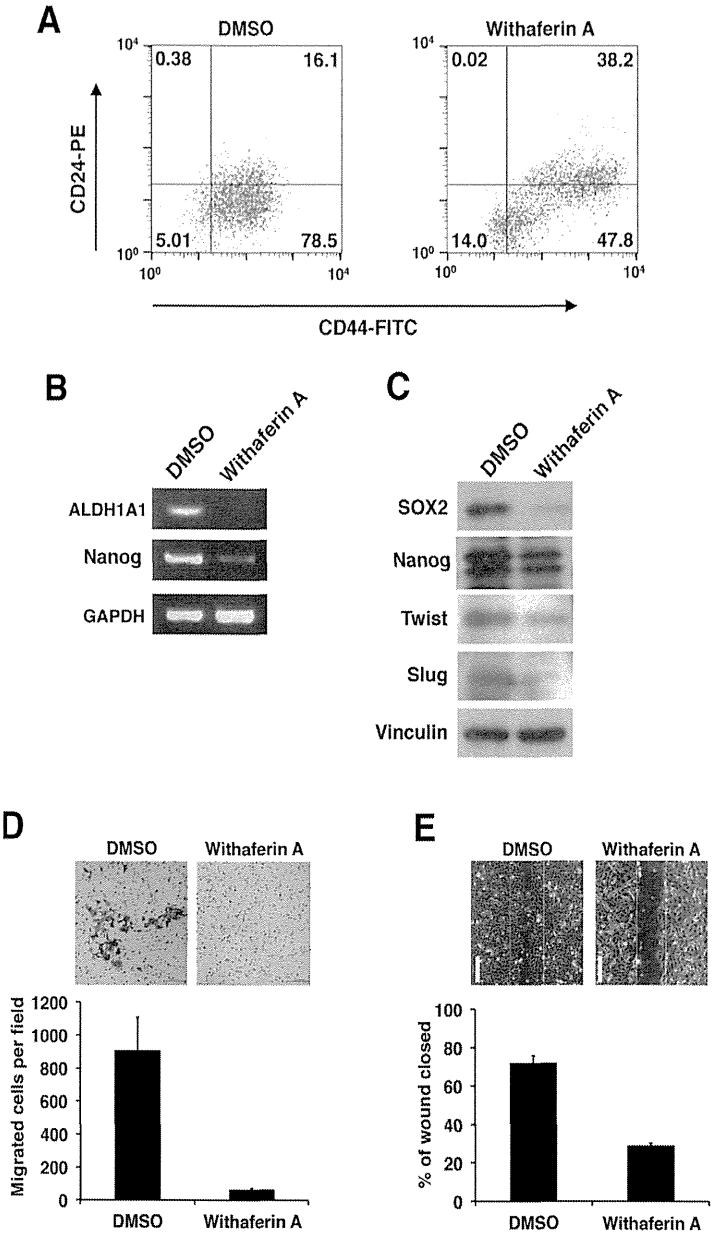

Figure 5: Withaferin A suppresses the CSC properties of iCSCL-10A cells. (A) Flow cytometric analysis of CD44 and CD24 expression in iCSCL-10A cells treated for 48 hrs with DMSO (control) or WA (1 μM). The numbers indicate the percentage of each subpopulation according to the CD44/CD24 expression profile. (B) Semi-quantitative PCR for ALDH1A1 and Nanog in iCSCL-10A cells treated for 48 hrs with DMSO or 1μM WA. Glyceraldehyde-3-phosphate dehydrogenase (GAPDH) expression was analyzed as a control. (C) Immunoblotting of stem cell and EMT marker proteins in iCSCL-10A cells treated for 48 hrs with DMSO or 1μM WA. Vinculin was used as a loading control. (D) Cell invasion assays were performed using chemotaxis chambers in transwell tissue culture dishes as described in the Materials and methods. After 48 hrs of treatment with DMSO or 1μM WA, iCSCL-10A cells were seeded in transwells. Representative microscopic fields are shown (upper). Invasive cells were counted and transwells were scored in triplicates. The mean values ± SD were calculated from three independent experiments (lower). (E) Effects of WA on wound healing. Confluent monolayers of iCSCL-10A cells were treated for 48 hrs with DMSO or 1 μM WA and a wounded was made using a pipette tip. After 6 hrs, the cells were fixed, images were captured and wound closure was scored using ImageJ software. Phase contrast microscopy images of the cells are shown (upper). Values represent the mean ± SEM (n = 3, lower). Scale bar, 1 mm.

senescence-associated marker γH2AX, a phosphorylated form of the histone variant H2AX [27]. We detected large phosphorylated H2AX foci in the WA treated cells but not in the DMSO-treated cells (Figure 7B). However, DNA damage response was not increased upon WA treatment as revealed by comet assay (Figure 7C) [28]. These results strongly indicate that the abrogation of CSC properties in iCSCL-10A cells is mediated by WA-induced senescence.

The expression pattern of cell cycle regulatory proteins was examined in WA-treated cells. There was a

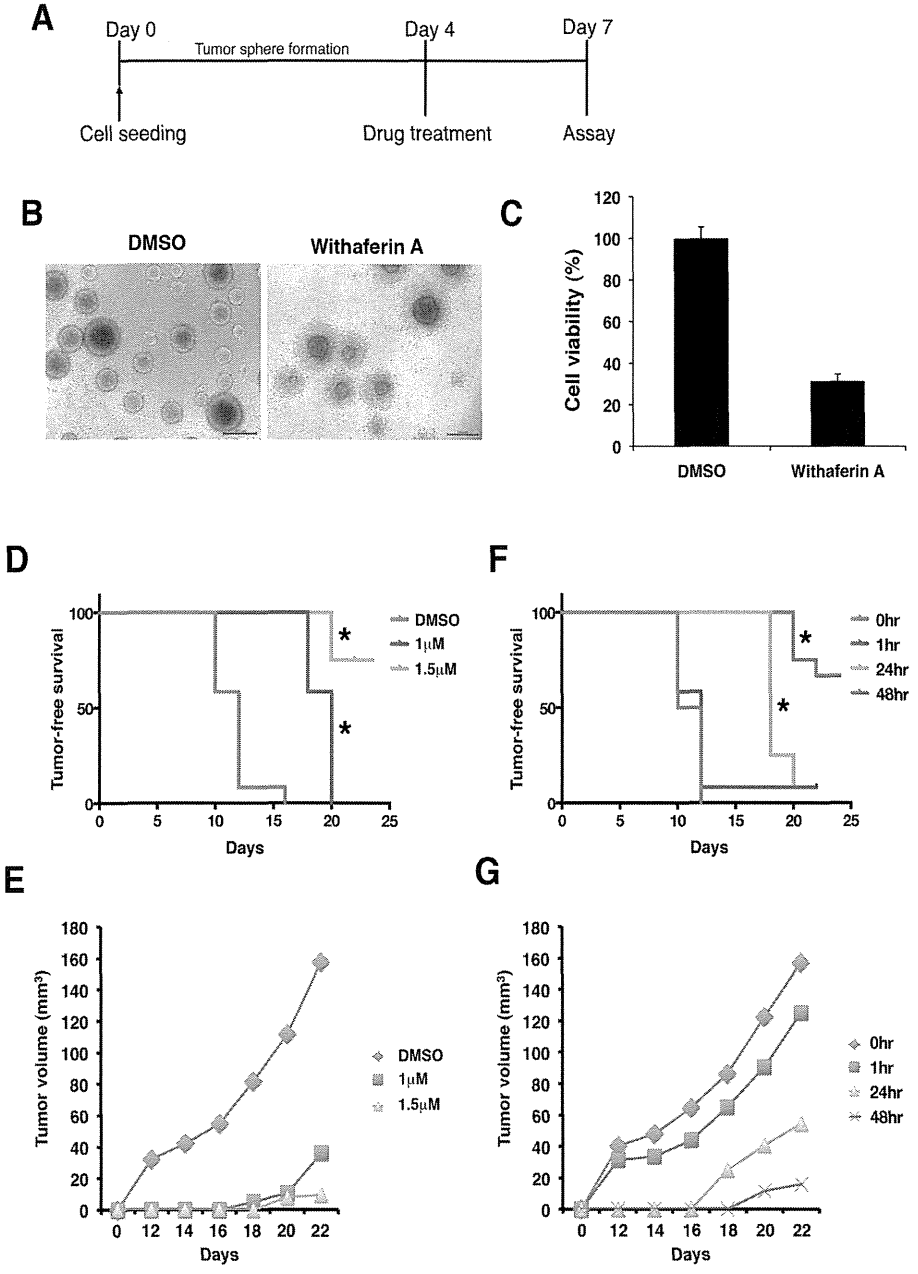

Figure 6: Withaferin A disrupts microenvironment and tumorigenicity of iCSCL-10A cells. (A-C) Time schedule of the experiment (A). iCSCL-10A cells were dissociated and then cultures for 4 days to form spheres in ultra-low attachment surface plates followed by the treatment of WA for another 3 days. At 7 days, cell viability was monitored by CellTiter-Glo™ Luminescent Cell Viability Assay (C). Values represent the mean ± SEM (n = 3). Phase contrast images of tumor spheres (B). (D, E) iCSCL-10A cells were pre-treated with the indicated concentrations of WA for 72 hrs, and the tumor seeding ability of the cells was assessed by injecting $1x10^6$ cells into nude mice. The tumor initiation ability per injection was monitored at different concentrations. Kaplan–Meier tumor-free survival curves mice receiving each cell types after injection at day 0. Statistically significant differences were observed between DMSO v.s. 1 mM and DMSO v.s. 1.5 mM, respectively (*, $P<0.01$) (D). Tumor size was monitored with by external caliper at indicated time points (E). Data represent means of 12 mice per condition. (F, G) iCSCL-10A cells were treated with 1.5 μM of WA for the indicated amount of time. WA treated cells ($1x10^6$ cells) were then injected subcutaneously into nude mice and the tumor initiating ability of the cells was then monitored over time. Tumor-free survival (F) and tumor size (G) was monitored as in (D) and (E). Statistically significant differences were observed between 0 hr v.s. 24 hr and 0 hr v.s. 48 hr, respectively (*, $P<0.01$). Data represent means of 12 mice per condition.

prominent increase in the expression of $p21^{Cip1}$ following treatment with WA, whereas p53 protein levels remained largely unchanged (Figure 7D). $p16^{Ink4a}$ expression was not observed due to deletion of INK4A/ARF locus in parental MCF-10A cells (Figure 7D) [29]. Cyclin B protein expression was markedly increased at the early time points but was suppressed after 24 hrs while cyclin D1 was increased at 48 hrs, which was further indicative of cellular senescence [28, 30]. It was shown that the activation of mitogenic pathways such as mammalian

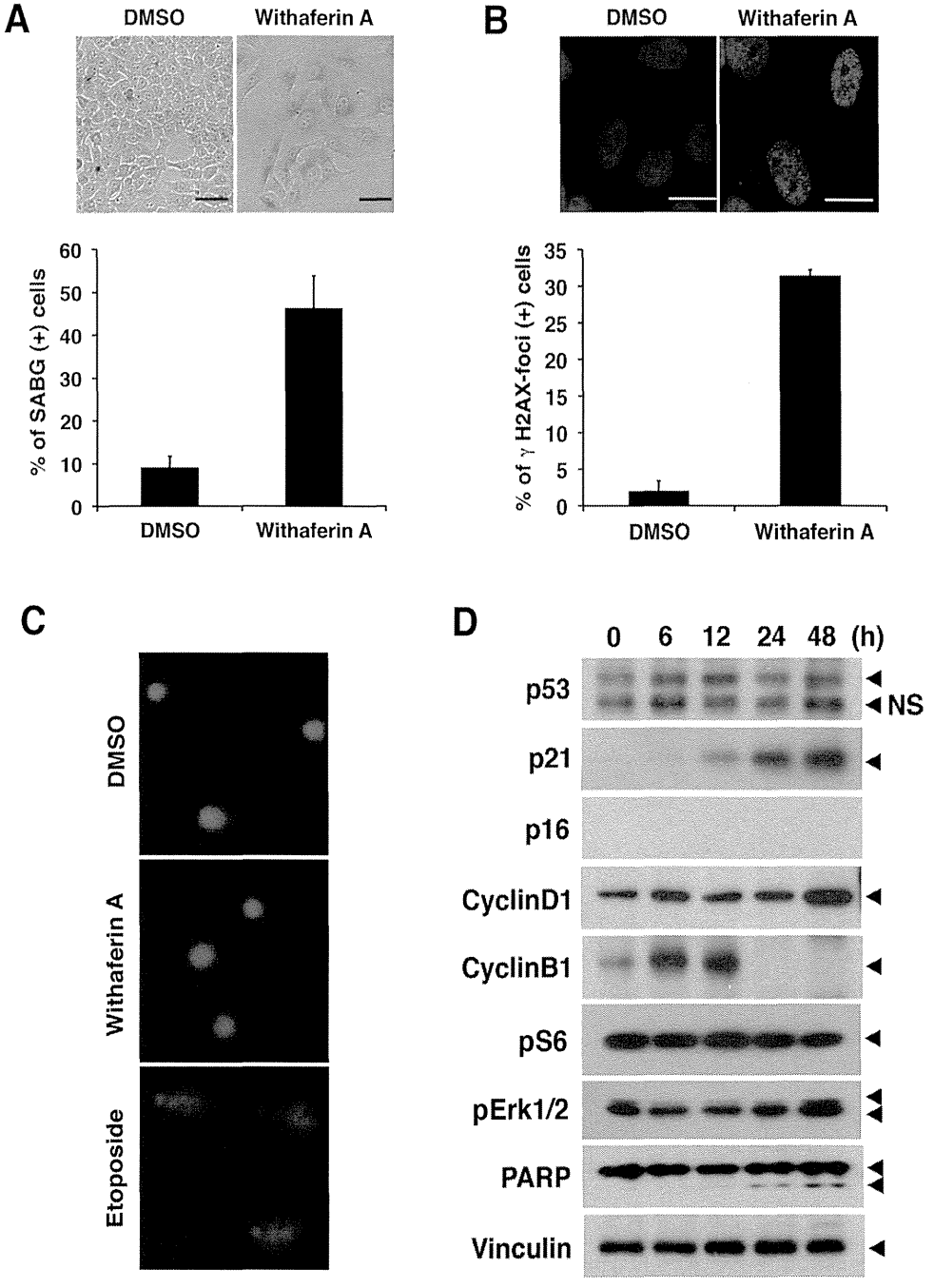

Figure 7: Withaferin A induces cellular senescence and increases $p21^{Cip1}$ expression in iCSCL-10A cells. (A) iCSCL-10A cells were treated with DMSO or 1μM of WA for 48 hrs and then stained for senescence-associated b-galactosidase (SABG). Phase contrast microscopy images of the cells are shown (upper). Scale bar, 100 mm. Bars indicate the percentage of SABG-positive cells for each condition and the data shown indicate mean ± SEM (n = 3, lower). One hundred cells per condition were counted and scored. (B) Immunofluorescent analysis of phospho-Histone H2A.X in iCSCL-10A cells treated with DMSO or 1μM of WA for 48 hrs. Nuclei were counterstained with DAPI. Phase contrast microscopy images of the cells are shown (upper). Scale bar, 100 mm. The number of phospho-Histone H2A.X cells was calculated and scored for three independent experiments (lower). Data shown are the mean ± SEM. One hundred cells per condition were counted and scored. (C) Cells were treated as in (B) and subjected to single-cell electrophoresis under denaturing conditions (comet assay). As a positive control, cells treated with10 μg/ml etoposide for 1 hr. (D) Immunoblotting of cell cycle related proteins in iCSCL-10A cells treated with 1 μM of WA at the indicated time points. Vinculin was used as a loading control.

target of rapamycin (mTOR) or mitogen-activated protein kinase (MAPK)/mitogen-activated/extracellular signal-regulated kinase (MEK) drives geroconversion from cell cycle arrest to senescence [30, 31]. Indeed, both phosphorylated S6 ribosomal protein (pS6) as a marker of mTOR and phosphorylated extracellular signal-regulated

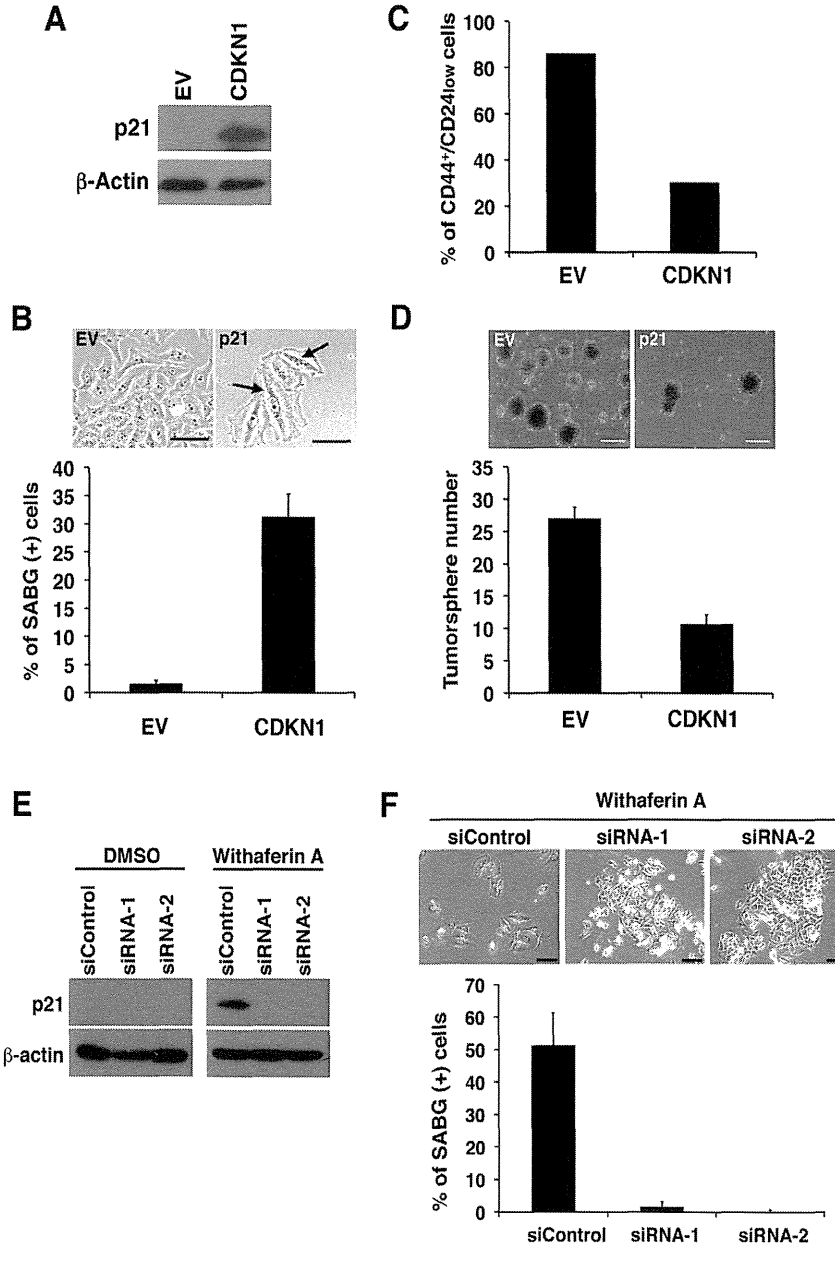

Figure 8: p21^{Cip1} suppresses CSC properties and induces cellular senescence of iCSCL-10A cells. (A) Whole cell lysates from iCSCL-10A cells transduced with the cyclin-dependent kinase inhibitor 1 (CDKN1) encoding p21^{Cip1} or empty vector (EV) control retrovirus were subjected to immunoblotting for the expression of the indicated proteins. β-Actin was used as a loading control. (B) CDKN1-transduced iCSCL-10A cells were stained with senescence-associated β-galactosidase staining (SABG). Phase-contrast microscopy images of the cells are shown (upper). Arrows indicate positive staining shown in blue. Scale bar, 200 mm. The graph shows the percentage of SABG-positive cells for each condition (lower). Data shown indicate the mean ± SEM (n=3). (C) Flow cytometic analysis for the expression of CD44 and CD24 in iCSCL-10A cells transduced with CDKN1 or empty vector (EV). The graph shows the frequency of CD44^{+}CD24^{low} cells in each of the culture conditions. (D) CDKN1 transduction abrogates the tumor sphere-forming ability of iCSCL-10A cells. Phase-contrast microscopy images of tumor spheres produced by iCSCL-10A cells transduced with CDKN1 or empty vector (EV) (upper). Data shown indicate the number of tumor spheres (means ± SEM, n=3, lower). (E, F) iCSCL-10A cells were transfected with p21^{Cip1}-siRNA for 48 hrs and then treated with 1μM WA for another 48 hr. Expression of p21Cip1 was assessed by immunoblot analysis (E). β-Actin was used as a loading control. Cells were stained with senescence-associated β-galactosidase staining (SABG). Phase contrast microscopy images of the cells are shown (upper). The graph shows the percentage of SABG-positive cells for each condition (lower). Data shown indicate the mean ± SEM (n=3) (F).

kinase (pErk1/2), as a marker of MAPK activity, were highly expressed in WA-treated cells during the course of senescence (Figure 7D). Moreover, there was no prominent cleavage of PARP (Figure 7D), strongly suggesting that the cells underwent senescence rather than apoptosis.

Ectopic $p21^{Cip1}$ expression largely recapitulates WA treatment in iCSCL-10A cells

In our iCSCL-10A cells, WA induced $p21^{Cip1}$ during the course of cellular senescence. In previous studies, expression of $p21^{Cip1}$ was tightly linked to cellular senescence [28, 32]. Therefore we evaluated whether $p21^{Cip1}$ played a role in WA-induced senescence and resultant abrogation of CSC tumorigenicity. To test this hypothesis, iCSCL-10A cells were transduced with the cyclin-dependent kinase inhibitor 1 (CDKN1) encoding $p21^{Cip1}$ using a retrovirus vector followed by selection with puromycin. Immunoblot analysis confirmed the stable expression of the ectopic $p21^{Cip1}$ in CDKN1-transduced cells (Figure 8A). CDKN1-transduced cells, but not control vector transduced cells, exhibited a flattened, enlarged, and heterogeneous cell morphology which was characteristic of cells in senescence (Figure 8B). These cells also expressed SABG, which was not observed among the control vector transduced cells (Figure 8B). Concomitantly, the $CD44^{+}CD24^{low}$ fraction within the CSC population was significantly reduced in the CDKN1-transduced cells (Figure 8C). Furthermore, CDKN1 transduction significantly reduced the rate of tumor sphere formation (Figure 8D).

On the contrary, the targeted depletion of endogenous $p21^{Cip1}$ by two different forms of siRNA prominently prohibited the WA-induced cellular senescence in iCSCL-10A cells as revealed by SABG staining in line with the suppression of WA-induced $p21^{Cip1}$ expression (Figure 8E, F). Taken together these results indicate that the expression of $p21^{Cip1}$ can abrogate the CSC properties of iCSCL-10A cells through the induction of cellular senescence.

DISCUSSION

In our current study, we developed and used an *in vitro* CSC-like model for the identification and characterization of novel agents targeting CSCs based on phenotypic properties. Several recent studies have attempted to use cell sorting to enrich a subpopulation of cancer cell lines as a potential CSC-like model [33]. However, a major limitation of these studies is the use of cell surface markers that may or may not be restricted to CSCs, and in some cases may be improved when combined with other properties [34]. Our current approach for creating a CSC-like cell population to assay the biological functions of CSCs sought to overcome these limitations by utilizing an iPSC technology for cellular reprogramming and subsequent partial differentiation of immortalized human mammary epithelial cells [24]. Although our technique manipulates iPS-like cells with further differentiation and transformation, the cells express CSC markers and retain the ability to differentiate into multiple lineages of cancer cells following *in vivo* transplantation into immunosuppressed mouse [22]. Forming the self-niche, cells can be maintained in regular cell culture medium without the need for co-culturing feeder cells to maintain the stemness. Our CSC-like model system improves the ease of characterization of cancer stem cells by enabling the examination of CSC-specific functions, such as self-renewal and tumor-initiating properties.

In our current study, we utilized three different assays, cell viability, tumor sphere formation and differentiation assays. Using our approach, we directly analyzed stemness and tumorigenic properties of CSC-like cells by monitoring their phenotypic features. WA was identified as a potential anti-CSC compound using our assay system, and was further validated with subsequent biological analyses. In fact, WA abrogated the maintenance of stemness and tumorigenicity via the induction of cellular senescence. Given the selectivity of our assay, future studies may be performed to identify additional compounds that prohibit CSC properties in large-scale analyses. In this regard, our approach would be useful not only for the identification of new targets for cancer therapy but also to improve the understanding of molecular pathways involved in the maintenance of CSCs.

We demonstrate here that WA can abrogate the tumorigenicity of CSC-like cells. WA is a steroidal lactone that is extracted from traces in all parts of Withania somnifera except its leaves [35]. Withania somnifera is one of the most ancient herbs that is used as a medicine and a dietary supplement [26]. Several previous studies illustrated the anti-cancer activity of WA both *in vitro* and *in vivo* [36, 37]. In fact, WA has been shown to induce apoptosis of human leukemia cells via inhibition of JNK and AKT signaling as well as inhibition of NF-κB activity [38]. WA also inhibited the growth of breast cancer cells by reducing the levels of Notch family proteins in MCF-7 and MDA-MB-231 cells [39]. WA has been also shown to induce mitotic catastrophe and growth arrest in prostate cancer cells [40]. These results indicate that WA may target distinct signaling molecules for its anti-cancer activity depending on the type of cancer cell. Notably, Kim et al. recently reported that WA treatment inhibited the mammosphere formation in MCF-7 and SUM159 human breast cancer cell lines as well as mammary epithelial cells derived from MMTV-neu mice [41]. In addition to this, we here revealed a distinct function of WA to target and disrupt self-renewal pathways of CSC via inducing $p21^{Cip1}$ and suppressing Twist thereby inducing

cellular senescence program possibly via cell cycle arrest and subsequent geroconversion (Figure 9). An improved understanding of the molecular link between WA and its regulation of CSC properties as revealed by in the current study may shed new light on the molecular signature of CSCs. Moreover, the identification of WA as a novel drug that targets CSCs may validate the feasibility of our assay system for anti-CSC drug discovery.

We show here that $p21^{Cip1}$ plays a crucial role in the abrogation of the malignant properties of CSCs via the induction of senescence. $p21^{Cip1}$ is a potent cyclin-dependent kinase (CDK) inhibitor that functions as a downstream effector of tumor suppressors including p53 and FOXO1 [32, 42]. Recent reports indicated crucial roles of $p21^{Cip1}$ not only in cell cycle regulation but also in the maintenance of normal and cancer stem cells. In the absence of $p21^{Cip1}$, hematopoietic stem cell proliferation and their absolute number were increased under normal homeostatic conditions [43]. Therefore, $p21^{Cip1}$ is regarded as a molecular switch governing the entry of stem cells into the cell cycle, and in its absence, increased cell cycling leads to stem cell exhaustion. $p21^{Cip1}$ has been also shown to attenuate Ras- and c-Myc-dependent breast tumor epithelial-mesenchymal transition and cancer stem cell gene expression *in vivo* [44]. Our current study also uncovered that $p21^{Cip1}$ plays a crucial role for cellular senescence in iCSCL-10A cells there by leading to the abrogation of their tumor-initiating properties. Moreover, constitutive activation of mTOR and/or MEK signaling also contributes to the geroconversion of iCSCL-10A cells toward cellular senescence [28, 30].

Activation of the senescence program in cancer cells is an attractive approach for the treatment of cancer [45]. In fact, cellular senescence has been recognized as a critical process in mammalian cells for the suppression of tumorigenesis and malignant transformation [46]. It is now clear that cellular senescence is a crucial anticancer mechanism that prevents the growth of cells at risk for neoplastic transformation into tumor initiating cells [47]. This crucial event can lead to the inhibition of metastatic dissemination, therapeutic resistance and generation of tumor cells with stem/progenitor cell properties [48, 49]. We clearly show here that WA promotes the senescence of CSC-like cells and limits their tumorigenicity and malignant characteristics. Indeed, only 48 hrs of WA treatment was sufficient to induce senescence-like morphological changes and SABG expression in iCSCL-10A cells. WA treatment increased the levels of $p21^{Cip1}$ in iCSCL-10A cells undergoing senescence. Targeted depletion of endogenous $p21^{Cip1}$ could block the WA-induced senescence. On the other hand, the ectopic expression of $p21^{Cip1}$ largely recapitulated the induction of senescence and loss of CSC properties observed in WA-treated iCSCL-10A cells. These results strongly suggest that $p21^{Cip1}$ plays a major role in inducing cellular senescence leading to the abrogation of the malignant nature in WA-treated CSCs.

WA suppressed the expression of EMT-related transcription factors including Twist. Twist plays a role in overcoming cellular senescence and in generating tumorigenic cancer stem cells [50, 51]. Indeed, Twist can abrogate oncogene-induced senescence and triggers epithelial-mesenchymal transition (EMT). Overexpression of Twist was shown to completely abrogate $p16^{Ink4a}$ and $p21^{Cip1}$ induction in Ras-iuduced premature senescence [52], suggesting that Twist is important for overriding cellular senescence in cooperation with oncogenes [53]. In our current study, WA strongly suppressed the expression of Twist which was in line with its induction of $p21^{Cip1}$. EMT is a process that is closely associated with the

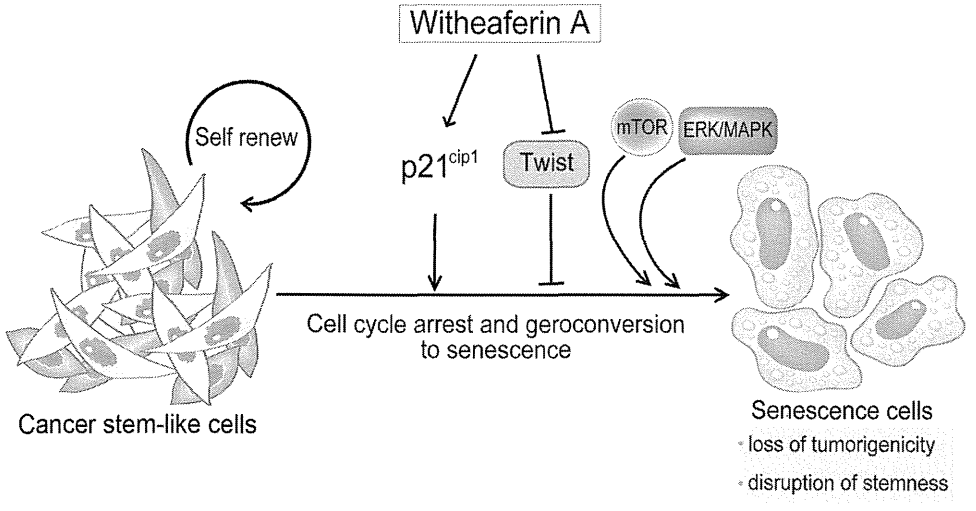

Figure 9: Withaferin A induces cellular senescence and prevents tumor initiating ability in CSC-like cells. Schematic presentation depicting how Withaferin A (WA) can prevent CSC stemness and tumor progression. WA enhances $p21^{Cip1}$ expression and suppresses the expression of an EMT-related transcription factor Twist. This event initiates cellular senescence program in CSC-like cells. In addition, the persistent activation of mitogenic pathways such as mTOR and/or MAPK/MEK may drive geroconversion from cell cycle arrest to senescence. Consequently, WA can abrogate CSC properties including tumor-initiating ability.

acquisition of invasive properties in cancer progenitor or pre-cancerous cells [54]. Our current findings highlight the potential therapeutic benefits of WA treatment as a primary safe-guard system against malignant transformation, namely, the prevention of the EMT-mediated malignant conversion of pre-cancerous cells into invasive cancer stem-like cells via the activation of senescence program [55].

Herein, we developed a simple, easy, cost-effective, and highly reproducible assay system that is applicable to large-scale drug screenings. Our optimized drug screen for CSC differentiation and stemness provides excellent consistency and reproducibility for the complex biological process of CSCs. Furthermore, this drug screen can be applied to a larger number of compounds to determine more selective and effective inhibitors of CSCs. This current approach holds great promise for future development of novel drugs to eliminate CSC and hopefully provide a complete cure for tumors.

MATERIALS AND METHODS

Cell culture

iCSCL-10A cells were generated and maintained as described previously [22]. Cells were cultured in Dulbecco's Modified Eagle's medium (DMEM) supplemented with 10% FBS and 1% penicillin/ streptomycin.

Chemicals

Phytochemical compounds library used in this study were purchased from TOKIWA PYTOCHEMICAL Co., Ltd (Chiba, Japan). Chemicals were diluted in DMSO to 10 mM without further purification.

Alkaline Phosphatase assay

iCSCL-10A cells ($5x10^3$ cells/well) were plated in 100 ml/well in 96-well plates. After 24 hrs, 1 mM of each compound was added to the appropriate wells. Alkaline Phosphatase (ALP) activity was measured after 48 hrs using the TRACP & ALP Assay Kit (TaKaRa, Shiga, Japan). For microscopic examination, cells were stained using the VECTOR Red Alkaline Phosphatase Substrate Kit (VECTOR Laboratories, Burlingame, CA) according to the manufacturer's protocol.

Cell Proliferation and Cytotoxicity Assays

Cell proliferation and cytotoxicity were evaluated using the Cell Counting Kit-8 (CCK-8) (Dojindo Molecular Technologies, Kumamoto, Japan). WST-8 reagent (2-(2-methoxy-4-nitrophenyl)-3-(4-nitrophenyl)-5-(2,4-disulfophenyl)-2H-tetrazolium) was added to the culture medium (1:10 dilution) and absorbance was measured at 450 nm.

RNA isolation and RT-PCR

Total RNA was extracted using TRIzol (Life Technologies, Grand Island, NY). cDNA synthesis was performed with ReverTraAce-α (Toyobo, Osaka, Japan) in accordance with the manufacturer's instructions. Real-time PCR was performed with Premix ExTaq (Takara Bio, Shiga, Japan) using the following primers: human ALDH1A1 fwd- TAAGCATCTCCTTACAGTCAC, rev-TGTTAAGTACTTCAAGAGTCAC; human GAPDH fwd- GTGGACCTGACCTGCCGTCT, rev-GGAGGAGTGGGTGTCGCTGT; human Nanog fwd-CAGCCCTGATTCTTCCACCAGTCCC, rev-TGGAAGGTTCCCAGTCGGGTTCACC.

Tumor sphere formation assay

Cells were seeded in 96-well ultra low-attachment surface plates (Corning) at a density of $5x10^3$ cells/well and cultured in serum-free DMEM-Ham's F12 nutrient mixture (1:1, v/v) supplemented with 5 mg/mL insulin, 0.5 mg/mL hydrocortisone, 2% B27, and epidermal growth factor (20 ng/ml).

Cell invasion assay

Cell invasion assays were performed using 24-well transwell inserts coated with 1 mg/ml matrigel (BD Biosciences, San Diego, CA). Invasive cells in the lower chamber were counted and scored in triplicate as described previously [22].

Wound healing assay

Cells were grown as a monolayer and a wound was made along the central axis of the plate using a pipette tip. The migration of cells into the wound was observed after 6 hrs in six randomly selected microscopic fields [56]. Wound closures were quantified using the image processing and analysis software program Image J 1.40g.

In vivo tumor formation assay

Cells were washed twice with antibiotic-free and serum-free cell culture medium and resuspended in 0.1 ml of serum-free culture medium. The cell suspension was mixed with an equal volume of Matrigel (BD Bioscience,

San Diego, CA) and then injected subcutaneously into 6-week-old BALB/c nude mice (CLEA Japan, Tokyo, Japan; N = 12 per condition). All animal experiments were performed under the guidelines and permission of Animal Use Protocol of Yokohama City University.

Statistical analysis

Kaplan-Meier's method with log-rank test and Gehan-Breslow-Wilcoxon test was used to assess the differences among the samples. GraphPad Prism 6 (GraphPad Software, La Jolla, CA) was used for this purpose. A value of $P<0.01$ was considered statistically significant.

Comet assay

Comet assay was performed using CometAssay kit (Trevigen Inc., Gaithersburg, MD) according to the manufacturer's instructions.

Immunostaining

For immunostaining, cells were fixed with 4% paraformaldehyde (PFA) for 15 min at 4°C, washed with PBS, and then permeabilized using 0.1% Triton X-100 before blocking with 5% goat serum in 0.1% BSA. Fixed cells were incubated with primary antibodies diluted in 0.1% BSA for 1 hr at room temperature followed by secondary antibody Alexa 488 or 568-conjugated anti-IgG (Life Technologies) as described previously [57].

Antibodies

The primary antibodies used in this study were as follows: anti-phospho-H2A.X and anti-Sox2 (Millipore, Billerrica, MA, USA), anti-p53 and anti-PARP (Cell Signaling Technology, Beverly, MA), anti-p21, anti-Slug and anti-Twist (Santa Cruz Biotechnology, Dallas, TX), anti-p16 and anti-Cyclin B1 (BD Biosciences, San Diego, CA), anti-Cyclin D1 (MBL International, Nagoya, Japan), anti-Nanog (ReproCELL, Yokohama, Japan), anti-b-actin and anti-Vinculin (SIGMA-Aldrich, St. Louis, MO).

ACKNOWLEDGEMENTS

We thank K Miyakawa, Y Watanabe, N Ikawa, H Nishikawa and N Kasuga for their excellent technical assistance. This work was supported in part by Creation of Innovation Centers for Advanced Interdisciplinary Research Areas Program and grant-in-aid from the Ministry of Education, Culture, Sports, Science and Technology of Japan (to A. R. and M. N.).

CONFLICT OF INTEREST

The authors state no conflict of interests.

REFERENCES

1. Clevers H. The cancer stem cell: premises, promises and challenges. Nat Med. 2011; 17(3):313-319.
2. Visvader JE and Lindeman GJ. Cancer stem cells in solid tumours: accumulating evidence and unresolved questions. Nat Rev Cancer. 2008; 8(10):755-768.
3. Alison MR, Lim SM and Nicholson LJ. Cancer stem cells: problems for therapy? J Pathol. 2011; 223(2):147-161.
4. Hanahan D and Weinberg RA. Hallmarks of cancer: the next generation. Cell. 2011; 144(5):646-674.
5. Dean M, Fojo T and Bates S. Tumour stem cells and drug resistance. Nat Rev Cancer. 2005; 5(4):275-284.
6. Bao S, Wu Q, McLendon RE, Hao Y, Shi Q, Hjelmeland AB, Dewhirst MW, Bigner DD and Rich JN. Glioma stem cells promote radioresistance by preferential activation of the DNA damage response. Nature. 2006; 444(7120):756-760.
7. Liu S and Wicha MS. Targeting breast cancer stem cells. J Clin Oncol. 2010; 28(25):4006-4012.
8. Sundberg SA. High-throughput and ultra-high-throughput screening: solution- and cell-based approaches. Curr Opin Biotechnol. 2000; 11(1):47-53.
9. Wilding JL and Bodmer WF. Cancer cell lines for drug discovery and development. Cancer Res. 2014; 74(9):2377-2384.
10. Singh AK, Arya RK, Maheshwari S, Singh A, Meena S, Pandey P, Dormond O and Datta D. Tumor heterogeneity and cancer stem cell paradigm: Updates in concept, controversies and clinical relevance. Int J Cancer. 2014.
11. Scaffidi P and Misteli T. In vitro generation of human cells with cancer stem cell properties. Nat Cell Biol. 2011; 13(9):1051-1061.
12. Kao CY, Oakley CS, Welsch CW and Chang CC. Growth requirements and neoplastic transformation of two types of normal human breast epithelial cells derived from reduction mammoplasty. In Vitro Cell Dev Biol Anim. 1997; 33(4):282-288.
13. Al-Hajj M, Wicha MS, Benito-Hernandez A, Morrison SJ and Clarke MF. Prospective identification of tumorigenic breast cancer cells. Proc Natl Acad Sci U S A. 2003; 100(7):3983-3988.
14. Singh SK, Clarke ID, Terasaki M, Bonn VE, Hawkins C, Squire J and Dirks PB. Identification of a cancer stem cell in human brain tumors. Cancer Res. 2003; 63(18):5821-5828.
15. Charafe-Jauffret E, Ginestier C, Iovino F, Wicinski J, Cervera N, Finetti P, Hur MH, Diebel ME, Monville F, Dutcher J, Brown M, Viens P, Xerri L, Bertucci F, Stassi G, Dontu G, et al. Breast cancer cell lines contain functional